

FAMILY OF INVARIANT CANTOR SETS AS ORBITS OF DIFFERENTIAL EQUATIONS. II: JULIA SETS

YI-CHIUAN CHEN*, TOMOKI KAWAHIRA†, HUA-LUN LI‡, AND JUAN-MING YUAN§

Abstract. The Julia set of the quadratic map $f_\mu(z) = \mu z(1 - z)$ for μ not belonging to the Mandelbrot set is hyperbolic, thus varies continuously. It follows that a continuous curve in the exterior of the Mandelbrot set induces a continuous family of Julia sets. The focus of this article is to show that this family can be obtained explicitly by solving the initial value problem of a system of infinitely coupled differential equations. A key point is that the required initial values can be obtained from the anti-integrable limit $\mu \rightarrow \infty$. The system of infinitely coupled differential equations reduces to a finitely coupled one if we are only concerned with some invariant finite subset of the Julia set. Therefore, it can be employed to find periodic orbits as well. We conduct numerical approximations to the Julia sets when parameter μ is located at the Misiurewicz points with external angle $1/2$, $1/6$, or $5/12$. We approximate these Julia sets by their invariant finite subsets that are integrated along the reciprocal of corresponding external rays of the Mandelbrot set starting from the anti-integrable limit $\mu = \infty$. When μ is at the Misiurewicz point of angle $1/128$, a 98-period orbit of prescribed itinerary obtained by this method is presented, without having to find a root of a 2^{98} -degree polynomial. The Julia sets (or their subsets) obtained are independent of integral curves, but in order to make sure that the integral curves are contained in the exterior of the Mandelbrot set, we use the external rays of the Mandelbrot set as integral curves. Two ways of obtaining the external rays are discussed, one based on the series expansion (the Jungreis-Ewing-Schober algorithm), the other based on Newton's method (the OTIS algorithm). We establish tables comparing the values of some Misiurewicz points of small denominators obtained by these two algorithms with the theoretical values.

Key words. Julia set, Mandelbrot set, external ray, anti-integrable limit

AMS subject classifications. 37F10, 37F45, 37F50

1. Introduction. A function f defined on an open set $V \subseteq \bar{\mathbb{C}}$ is called *holomorphic* (or *complex analytic*) if the first derivative $z \mapsto Df(z)$ is defined and continuous as a function of V . It is known that every complex quadratic polynomial map $z \mapsto az^2 + bz + d$ ($a, b, d \in \mathbb{C}$, $a \neq 0$) can be put into a normal form

$$q_c : z \mapsto z^2 + c, \quad z, c \in \mathbb{C}, \quad (1.1)$$

by an affine change of coordinates: $z \mapsto az + b/2$ with $c = ad - b^2/4 + b/2$. Another well-known normal form is the logistic map

$$f_\mu : z \mapsto \mu z(1 - z), \quad z, \mu \in \mathbb{C}, \quad (1.2)$$

which is affinely conjugate to q_c via the conjugacy

$$h : z \mapsto -\mu z + \mu/2 \quad (\text{so that } h \circ f_\mu \circ h^{-1} = q_c) \quad (1.3)$$

with

$$c = \mu(2 - \mu)/4 \quad (\mu \neq 0). \quad (1.4)$$

Hence, we can freely employ either form (1.1) or (1.2) for investigation of quadratic holomorphic maps, according to which one is convenient.

For the preliminary, in suitable places of this paper, we shall recall some definitions and theorems in the complex dynamical systems. The reader may consult, for example, references [3, 6, 10, 14, 27, 28] for further details. A collection \mathcal{F} of holomorphic maps from a domain $V \subseteq \bar{\mathbb{C}}$ to another $U \subseteq \bar{\mathbb{C}}$ is

*Institute of Mathematics, Academia Sinica, Taipei 11529, Taiwan (YChen@math.sinica.edu.tw).

†Graduate School of Mathematics, Nagoya University, Nagoya 464-8602, Japan (kawahira@math.nagoya-u.ac.jp).

‡Department of Applied Mathematics, Chung Hua University, Hsinchu 300, Taiwan (hualun@chu.edu.tw).

§Department of Applied Mathematics, Providence University, Shalu, Taichung 433, Taiwan (jmyuan@pu.edu.tw).

called *normal* if every infinite sequence of maps from \mathcal{F} contains a subsequence that converges uniformly on compact subsets of V in the standard spherical metric $ds = 2|dz|/(1 + |z|^2)$. The *Fatou set* for a nonconstant holomorphic map $f : V \rightarrow V$, $V \subseteq \mathbb{C}$, is the set of points $\hat{z} \in V$ such that the forward iterates $(f^n)_{n \geq 0}$ is a normal family on some neighborhood of \hat{z} . The *Julia set*, denoted by $J(f)$, is the complement of the Fatou set. Since q_c and f_μ are polynomials, their Julia sets can be characterized in a simpler manner. By $K(q_c)$ we denote the *filled Julia set* of the map q_c ,

$$K(q_c) := \{z \mid q_c^n(z), n \geq 0, \text{ is bounded}\},$$

then the Julia set $J(q_c)$ of q_c is the boundary of the filled Julia set,

$$J(q_c) := \partial K(q_c).$$

The Julia set $J(q_c)$ may also be characterized as the closure of the set of repelling periodic points of q_c . These three definitions of Julia set $J(q_c)$ are equivalent. The celebrated *Mandelbrot set* [5, 24] for q_c is defined to be

$$M_c := \{c \mid q_c^n(0), n \geq 0, \text{ is bounded}\}.$$

Analogously, we use $K(f_\mu)$, $J(f_\mu)$, and

$$M_\mu := \{\mu \mid f_\mu^n(1/2), n \geq 0, \text{ is bounded}\}$$

to denote the filled Julia set, the Julia set, and the Mandelbrot set of f_μ , respectively. A conspicuous feature is that the orbit of the critical point plays a crucial role in determining the topological structure of the Julia set.

THEOREM 1.1 ([3, 6, 14, 27]). *$K(f_\mu)$ and $J(f_\mu)$ are connected if $\mu \in M_\mu$, whereas $K(f_\mu)$ is a Cantor set and is equal to $J(f_\mu)$ if $\mu \notin M_\mu$.*

One of the most important concepts in dynamical systems is the hyperbolicity, which we state in the current context as follows.

DEFINITION 1.2. *A rational map $f : \bar{\mathbb{C}} \rightarrow \bar{\mathbb{C}}$ is called hyperbolic if there exists a conformal metric ρ , defined on a neighborhood of its Julia set $J(f)$, such that*

$$\|f'(z)v\|_\rho > \|v\|_\rho \tag{1.5}$$

at every point $z \in J(f)$ for every nonzero v in the tangent space $T_z\bar{\mathbb{C}}$.

The classical result below is fundamental to this article.

THEOREM 1.3 ([3, 15]). *f_μ is hyperbolic if $\mu \notin M_\mu$.*

When parameter μ changes, the Julia set of f_μ changes accordingly. The Julia set for μ not belonging to the Mandelbrot set is hyperbolic, thus varies continuously (see for example [22, 25]). It follows that a continuous curve in the exterior of the Mandelbrot set induces a continuous family of Julia sets. In this paper, we are concerned with the visualization of this family. This family is in fact governed by an explicit form of infinitely coupled differential equations (see (3.3) below) that we obtained recently [9]. The paper [9] deals with real parameter $\mu \geq 4$, and it is natural to extend the study to its complex-counterpart. The geometric shape of Julia set can more or less be imagined for real $\mu > 4$. However, unless we see it, its shape for the complex valued μ is in general not possible to be imagined, particularly, when the parameter is near the boundary of the Mandelbrot set. Besides, unlike the real valued μ , we may have to specify integral curves so as to obtain the Julia sets for certain values of parameter μ . For instance, if we want to obtain the Julia set for certain μ near a Misiurewicz point, we need a curve on the parameter space starting from the anti-integrable limit $\mu = \infty$ and ending at that μ . (A point $c \in \partial M_c$ is called a *Misiurewicz point* if the orbit of 0 is strictly preperiodic, i.e. $q_c^n(0) = q_c^m(0)$ for some $n > m > 0$ but $q_c^n(0) \neq 0$ for all $n \geq 1$. For the concept of anti-integrability, we refer the reader to references [1, 7, 8, 23, 30].) But not

every curve can serve as an integral curve for (3.3) because it may have intersection with the Mandelbrot set. Therefore, we need a carefully selected curve that can avoid the jangled filaments of the Mandelbrot boundary and reach the destined μ . In this paper, we select the external rays (see Definition 2.2) of the Mandelbrot set to be our integral curves.

The external rays we actually select have rational external angles of even denominators. We choose such external rays due to the following two reasons. First, they terminate at the Misiurewicz points on the boundary of the Mandelbrot set (as stated in Theorem 2.4). It is known that $K(f_{\hat{\mu}})$ has no interior point thus equal to $J(f_{\hat{\mu}})$ when $\hat{\mu}$ is a Misiurewicz point. In addition, the filled Julia set coincides with the Julia set when μ is not located in the Mandelbrot set for f_{μ} . Douady [13] showed that the filled Julia set $K(f_{\mu})$ depends upper semi-continuously on μ in the Hausdorff topology, while the Julia set $J(f_{\mu})$ depends lower semi-continuously on μ . Thereby, our second reason is that, when $\hat{\mu}$ is a Misiurewicz point, we have $J(f_{\mu}) \rightarrow J(f_{\hat{\mu}})$ continuously in the Hausdorff topology as $\mu \rightarrow \hat{\mu}$ along an external ray that terminates at $\hat{\mu}$.

Hence, the continuous family of Julia sets $J(f_{\mu})$ when μ varies from infinity along an external ray of the Mandelbrot set M_{μ} to a Misiurewicz point can be realized as an orbit of the infinitely coupled differential equations (3.3) integrated along the external ray. This approach will bring some new insight into the study of complex dynamical systems.

By virtue of Theorem 3.2, the Julia set $J(f_{\mu})$ obtained by integrating (3.3) is in fact independent of the integral curve used; it depends only on the end point μ of the integral curve (the other end point is ∞). Therefore, if not taking the numerical rounding errors into account, to get a figure of the Julia set, we can concentrate on whether the external ray we shall choose will pass through μ within a given precision or not. In this paper, we use the OTIS algorithm [21], which is based on Newton's method, to obtain numerical data of the external rays. An error estimate for this algorithm is presented in Theorem 5.1.

There is another algorithm, based on the series expansion to obtain numerical data of external rays, due to Jungreis [20], Ewing and Schober [18]. The Jungreis-Ewing-Schober (JES) algorithm concerns finding the coefficients b_m of a series expansion, and the explicit formula $\hat{\Phi}^{-1}(w) := w + \sum_{m \geq 0} b_m w^{-m}$ sends the straight line $\{w \mid \arg(w) = \theta, |w| > 1\}$ from the complement $\mathbb{C} \setminus \mathbb{D}_1$ of the closed unit disc to the external ray of angle θ in the complement $\mathbb{C} \setminus M_c$ of the Mandelbrot set M_c . The JES algorithm is very easy to programme by computer. Another advantage is that a finite series of the expansion will send a straight line of angle θ in $\mathbb{C} \setminus \mathbb{D}_1$ to an approximation of the external ray of the same angle in $\mathbb{C} \setminus M_c$, thus with the help of a finite expansion the integral curves for (3.3) will practically be straight lines. See Remark 3.3 for the detail. However, the series converge very slow, especially near the boundary of the Mandelbrot set.

Table 5.1 lists landing points (see Definition 2.2) of some external rays of rational angles having small even denominators obtained by the JES and OTIS algorithms together with their theoretical values. It is apparent that the results by our OTIS programme match the theoretical values up to the seventh decimal place, whereas the same accuracy cannot be achieved by the JES algorithm even with one million terms of coefficients b_m . Hence, in this paper we utilize the OTIS programme to generate the needed numerical data for integral curves.

Incidentally, taking advantage of the one million coefficients, along with Gronwall's area formula we get a new upper bound for the area of the Mandelbrot set M_c . The area is less than 1.703927.

This paper is organized as follows. After this Introduction, we review in Section 2 how the external rays of the Julia sets and the Mandelbrot set are defined by means of the potential functions, and how these are relevant to partitioning the Julia set. Our itinerary codes for Julia sets are described in Section 3. In Theorem 3.2, we show that, in the exterior of the Mandelbrot set, all points in Julia set are originated from the anti-integrable limit and vice versa, and show how the unique point with a given itinerary code can be obtained by solving (3.3). Section 4 devotes to four examples of application of Theorem 3.2. We integrate (3.3) along the external rays of angles $1/2$, $1/6$, $5/12$, and present 2-D and 3-D animations as well as figures showing how the Julia sets (approximated by invariant subsets) vary along the rays. We

also demonstrate the power of using Theorem 3.2 to obtain periodic orbits by an example of period-98 orbit. A fairly detailed account of the JES and the OTIS algorithms for the external rays of the Mandelbrot set is drawn in Section 5. There, it shows that the integral curves we used in this paper are rather accurate.

2. Symbolic codings, potential functions and external rays. It is an elementary fact that the Julia set $J(q_c)$ is a Cantor set when $c \notin M_c$, thus, it is homeomorphic to the set Σ consisting of sequences of 0's and 1's,

$$\Sigma := \{e = \{e_0, e_1, e_2, \dots\} \mid e_n = 0 \text{ or } 1 \forall n \geq 0\}, \quad (2.1)$$

with the product topology. Actually, there exists a homeomorphism between them such that the following diagram commutes

$$\begin{array}{ccc} \Sigma & \xrightarrow{\sigma} & \Sigma \\ \downarrow & & \downarrow \\ J(q_c) & \xrightarrow{q_c} & J(q_c). \end{array}$$

In other words, the restriction of q_c to its Julia set is topologically conjugate to the Bernoulli shift σ on two symbols. The one-to-one correspondence between J_c and Σ implies that we can assign each point in the Julia set a *symbolic code*. But, there is no unique way to assign the code. One example of such a coding is the *itinerary code* or *itinerary sequence*. Below we give a brief exposition recalling the canonical potential function associated with the filled Julia set in order to see how an itinerary sequence is assigned and to introduce some notations as well.

Let

$$\beta = 1/c. \quad (2.2)$$

The dynamical behavior of q_c near infinity can be understood by making the substitution $\zeta = 1/z$ and considering the rational function

$$Q_\beta(\zeta) := \frac{1}{q_{1/\beta}(1/\zeta)} = \frac{\beta\zeta^2}{\beta + \zeta^2}.$$

For ζ small, it has a power series expansion of the form $Q_\beta(\zeta) = \zeta^2 - \zeta^4/\beta + \text{higher order terms}$. Because $\zeta = 0$ is a superattracting fixed point of Q_β (i.e. $Q'_\beta(0) = 0$), the associated Böttcher map ϕ_β defined by

$$\phi_\beta(\zeta) := \lim_{n \rightarrow \infty} \sqrt[n]{Q_\beta^n(\zeta)}$$

carries an open subset of the immediate basin $\mathcal{A}_0(0)$ of the fixed point 0 biholomorphically onto an open disc \mathbb{D}_r of radius r , $0 < r \leq 1$, centred at the origin. In addition, the function $\zeta \mapsto |\phi_\beta(\zeta)|$ extends uniquely to a continuous function $|\phi_\beta(\cdot)| : \mathcal{A}(0) \rightarrow [0, 1)$ on the entire basin of attraction of zero satisfying $|\phi_\beta(Q_\beta(\zeta))| = |\phi_\beta(\zeta)|^2$. If $\beta \in M_c^{-1}$, where

$$M_c^{-1} := \{1/c \mid c \in M_c\},$$

then $r = 1$ and $\phi_\beta^{-1}(\mathbb{D}_1) = \mathcal{A}(0) = \mathcal{A}_0(0)$, while if $\beta \notin M_c^{-1}$, then $r = \lim_{\zeta \rightarrow \infty} |\phi_\beta(\zeta)| < 1$ and $\phi_\beta^{-1}(\mathbb{D}_r) = \{\zeta \mid |\phi_\beta(\zeta)| < r\}$.

By virtue of the identity

$$\sqrt[n]{q_c^n(z)} = z \prod_{k=1}^n \sqrt[k]{1 + \frac{c}{(q_c^{k-1}(z))^2}}, \quad (2.3)$$

in the z -plane, the map $\hat{\phi}_c$ defined by the reciprocal

$$\begin{aligned}\hat{\phi}_c(z) &:= \frac{1}{\phi_{1/c}(1/z)} \\ &= \lim_{n \rightarrow \infty} \sqrt[2^n]{q_c^n(z)} \\ &= z \prod_{n \geq 1} \sqrt[2^n]{1 + \frac{c}{(q_c^{n-1}(z))^2}}\end{aligned}$$

maps biholomorphically from the open set $\{z \mid G_c(z) > G_c(0)\} \subseteq \mathbb{C} \setminus K(q_c)$ to the region $\mathbb{C} \setminus \bar{\mathbb{D}}_{\hat{r}} = \{w \mid \ln |w| > G_c(0)\}$, where $\hat{r} = |\hat{\phi}_c(0)| > 1$ and $G_c : \mathbb{C} \rightarrow [0, \infty)$, defined by

$$G_c(z) := \ln^+ |\hat{\phi}_c(z)| = \lim_{n \rightarrow \infty} \frac{1}{2^n} \ln^+ |q_c^n(z)|, \quad (\ln^+ |w| = \max\{\ln |w|, 0\})$$

is the *canonical potential function*, or *rate of escape function*, associated with the filled Julia set $K(q_c)$. Note that G_c is defined and continuous everywhere, satisfying $G_c(q_c(z)) = 2G_c(z)$, in particular, $G_c(z) = 0$ if $z \in K(q_c)$, and $G_c(z) > 0$ if $z \notin K(q_c)$. Also, note that if $c \in M_c$, then $G_c(0) = 0$, and that if $c \notin M_c$, then $G_c(0) > 0$. The map $\hat{\phi}_c$, which possesses properties

$$\hat{\phi}_c(q_c(z)) = \hat{\phi}_c(z)^2, \quad (2.4)$$

$$\hat{\phi}_c(z)/z \rightarrow 1 \text{ as } z \rightarrow \infty, \quad (2.5)$$

acts as a conjugacy between q_c on $\{z \mid G_c(z) > G_c(0)\}$ and $w \mapsto w^2$ on $\{w \mid \ln |w| > G_c(0)\}$.

DEFINITION 2.1. For $\theta \in \mathbb{R}/\mathbb{Z}$, define the external ray $\mathcal{R}(\theta; K(q_c))$ of angle θ of the filled Julia set $K(q_c)$ by

$$\mathcal{R}(\theta; K(q_c)) := \{\hat{\phi}_c^{-1}(re^{i2\pi\theta}) \mid |\hat{\phi}_c(0)| < r \leq \infty\}. \quad (2.6)$$

When $c \notin M_c$, the critical value $c \in \mathbb{C} \setminus K(q_c)$ has a well defined external angle, denoted by $l(c) \in \mathbb{R}/\mathbb{Z}$, given by $c = \hat{\phi}_c^{-1}(|\hat{\phi}_c(c)|e^{i2\pi l(c)})$. The ray $\mathcal{R}(l(c); K(q_c))$ has two preimages under q_c , $\mathcal{R}(l(c)/2; K(q_c))$ and $\mathcal{R}((l(c) + 1)/2; K(q_c))$. These two together with the origin separate $\bar{\mathbb{C}}$ into two disjoint open sets, say V_0 and V_1 . (See Figure 4.4 (a).) Let $U_0 = K(q_c) \cap V_0$ and $U_1 = K(q_c) \cap V_1$. These constitute a *Markov partition*. That is to say, for any one sided infinite sequence $(b_0, b_1, \dots) \in \Sigma$, there exists one and only one point $z \in K(q_c)$ with $q_c^i(z) \in V_{b_i}$ for every $i \geq 0$. However, there is ambiguity in determining which open set should be labeled by V_0 and which by V_1 . (See also Remark 3.4.) In the next section we shall define the itinerary sequences used in this paper for points in the Julia set $J(f_\mu)$. Our definition arises very naturally from the system's anti-integrable limit. (See Definition 3.1.)

Suppose $n \geq 0$, then $q_c^n(c)$ is a monic polynomial of degree 2^n in c . It is known that all zeros of $q_c^n(c)$ lie in M_c , and so one can define

$$\hat{\Phi}_n(c) := \sqrt[2^n]{q_c^n(c)} \quad (2.7)$$

in $\bar{\mathbb{C}} \setminus M_c$ by the branch $\hat{\Phi}_n(c) = c + O(1)$ as $c \rightarrow \infty$. It is easy to see that $|q_c^n(c)| > 2$ implies that $|q_c^{n+1}(c)| > |q_c^n(c)|$, and it turns out that $\hat{\Phi}_n$ is a holomorphic map of $\bar{\mathbb{C}} \setminus M_c$, and when restricted to the set $U_n := \{c \in \bar{\mathbb{C}} : |q_c^n(c)| > 2\}$ is bijective to $\bar{\mathbb{C}} \setminus \bar{\mathbb{D}}_{2^n\sqrt{2}}$. Since $U_n \subset U_{n+1}$, and $\bigcup_{n \geq 1} U_n = \bar{\mathbb{C}} \setminus M_c$, it follows immediately from the Carathéodory Kernel Convergence Theorem that the sequence $\hat{\Phi}_n$ converges as $n \rightarrow \infty$ uniformly on compact subsets of $\bar{\mathbb{C}} \setminus M_c$ to the function $\hat{\Phi}$ with $\hat{\Phi}(c) \equiv \hat{\phi}_c(c)$, which is biholomorphic from $\bar{\mathbb{C}} \setminus M_c$ to $\bar{\mathbb{C}} \setminus \bar{\mathbb{D}}_1$, and the inverse $\hat{\Phi}_n^{-1}$ converges to $\hat{\Phi}^{-1}$ uniformly on compact subsets of $\bar{\mathbb{C}} \setminus \bar{\mathbb{D}}_1$.

DEFINITION 2.2. For $\theta \in \mathbb{R}/\mathbb{Z}$, the set

$$\mathcal{R}(\theta; M_c) := \{\hat{\Phi}^{-1}(re^{i2\pi\theta}) \mid 1 < r \leq \infty\}$$

is called the external ray of angle θ of the Mandelbrot sets M_c . If $\lim_{r \rightarrow 1^+} \hat{\Phi}(re^{i2\pi\theta})$ exists, then this limit is called the landing point of the external ray $\mathcal{R}(\theta, M_c)$.

Remark 2.3. Adopted from [26], we also call an external ray of the Mandelbrot set a *parameter ray*, and call an external ray of the filled Julia set a *dynamic ray*.

The following theorem states that all rational parameter rays land at ∂M_c .

THEOREM 2.4 ([6, 14, 27, 28]). *If θ is rational, then $\mathcal{R}(\theta; M_c)$ lands at a point $c \in \partial M_c$. If θ has even denominator, c is a Misiurewicz point; if θ has odd denominator, q_c has a parabolic cycle.*

3. Continuation from the anti-integrable limit. In [9], we derived a system of infinitely coupled differential equations (the equation (3.3) below) that governs the behavior of orbit points in the Julia set $J(f_\mu)$ when μ is real and greater than 4. As a matter of fact, by following almost the same proof, it can be shown that the system governs $J(f_\mu)$ as long as μ does not belong to the Mandelbrot set M_μ . Briefly, it can be derived as follows. Providing $\epsilon = 1/\mu \neq 0$, then a sequence $\{z_n\}_{n \geq 0}$ is an orbit for the logistic map if and only if

$$z_{n+1} = \epsilon^{-1} z_n (1 - z_n). \quad (3.1)$$

Assume that each z_n depends C^1 on ϵ , taking derivative with respect to ϵ on both sides, then we have

$$-\epsilon \frac{d}{d\epsilon} z_{n+1} + (1 - 2z_n) \frac{d}{d\epsilon} z_n = z_{n+1}. \quad (3.2)$$

The differential-difference equation (3.2) further gives rise to the desired system of infinitely coupled differential equations

$$\frac{d}{d\epsilon} z_n = \sum_{N \geq 0} \epsilon^N \left(\prod_{k=0}^N (1 - 2z_{n+k})^{-1} \right) z_{n+1+N}. \quad (3.3)$$

The assumption of C^1 -dependence can be guaranteed by virtue of the C^1 -persistence of hyperbolic Julia set. By the hyperbolicity again, the sum of the infinite series in (3.3) can be bounded by geometric series thus is finite.

The crucial matter is how to solve (3.3). We shall treat it as the initial value problem, with initial values specified at $\epsilon = 0$. It has been shown in [8] that, as ϵ approaches zero, the set of bounded orbits $\{z_n^*(\epsilon)\}_{n \geq 0}$ of the map $f_{1/\epsilon}$ converges to the set Σ . This indicates that for every $n \geq 0$ there are exactly two possibilities for the initial condition: $z_n^*(0) = 0$ or $z_n^*(0) = 1$.

By means of (1.3), define

$$\mathcal{R}(\theta; K(f_\mu)) := h^{-1}(\mathcal{R}(\theta; K(q_c))).$$

From Section 2, the two external rays $\mathcal{R}(l(c)/2; K(f_{1/\epsilon}))$ and $\mathcal{R}((l(c) + 1)/2; K(f_{1/\epsilon}))$, which land at the point $z = 1/2$, divide the complex plane into two partitions, one containing the fixed point 0, the other containing the other fixed point $1 - \epsilon$.

DEFINITION 3.1. *Assume $z_{n+1} = f_{1/\epsilon}(z_n)$ for all $n \geq 0$. Suppose $\{z_n\}_{n \geq 0}$ is bounded and is bounded away from the two dynamic rays that land at the critical point $1/2$. Then, define its itinerary sequence $\{\alpha_n\}_{n \geq 0}$ in such a way that $\alpha_n = 0$ if z_n is located in the same partition as the fixed point 0 is and that $\alpha_n = 1$ if z_n is located in the same partition as the fixed point $1 - \epsilon$ is.*

Since for every $n \geq 0$ the solution $z_n^*(\epsilon)$ of (3.3) depends continuously on ϵ and has to be bounded away from the two dynamic rays, the itinerary sequence of $\{z_n^*(\epsilon)\}_{n \geq 0}$ is equal to $\{z_n^*(0)\}_{n \geq 0}$. This

means the itinerary sequences for the family (with respect to ϵ) of solutions $\{z_n^*(\epsilon)\}_{n \geq 0}$ do not change, all identical to $\{z_n^*(0)\}_{n \geq 0}$. Let the mapping $\{z_n^*(0)\}_{n \geq 0} \mapsto \{z_n^*(\epsilon)\}_{n \geq 0}$ be denoted by g_ϵ , and let the projection $(z_0, z_1, \dots) \mapsto z_0 \in \mathbb{C}$ be denoted by π . As was proved in [8] for the real-variable case, it can be shown that the following diagram commutes

$$\begin{array}{ccc} \Sigma & \xrightarrow{\sigma} & \Sigma \\ \pi \circ g_\epsilon \downarrow & & \downarrow \pi \circ g_\epsilon \\ J(f_{1/\epsilon}) & \xrightarrow{f_{1/\epsilon}} & J(f_{1/\epsilon}) \end{array}$$

provided that $\epsilon \notin M_\mu^{-1}$. (The “inside-out” Mandelbrot set M_μ^{-1} is defined by

$$M_\mu^{-1} := \{1/\mu \mid \mu \in M_\mu\}.$$

See Figure 4.4 (b).) In the diagram, the Julia set $J(f_{1/\epsilon})$ is obtained by

$$J(f_{1/\epsilon}) := \bigcup_{\{z_n^*(0)\}_{n \geq 0} \in \Sigma} \pi \circ g_\epsilon(\{z_n^*(0)\}_{n \geq 0}).$$

One advantage of the proof in [8] is that the conjugacy between Σ and $J(f_{1/\epsilon})$ comes automatically and can be realized explicitly as $\pi \circ g_\epsilon$. In fact, g_ϵ is realized as the solutions of the initial value problems for the infinitely coupled differential equations (3.3).

Once initial conditions $z_n^*(\epsilon = 0)$ for all $n \geq 0$ are given, the value of the solution $z_n^*(\epsilon)$ of (3.3) at $\epsilon = \hat{\epsilon} \in \bar{\mathbb{C}} \setminus M_\mu^{-1}$ depends only on $\hat{\epsilon}$, and in particular is independent of integral curves. Therefore, to determine the value of $z_n^*(\hat{\epsilon})$, we only need to make sure the integral curves that we employ do not intersect with the Mandelbrot set M_μ^{-1} . Because $\hat{\epsilon}$ may locate arbitrarily near ∂M_μ^{-1} , we have to specify an integral curve that can approach as close as possible to the boundary ∂M_μ^{-1} . This can be done if the integral curve is an external ray. To this end, we choose the rational external rays of M_μ^{-1} to be our integral curves.

In contrast to $\hat{\Phi}^{-1}$, the map Φ^{-1} defined by

$$\Phi^{-1}(w) := \frac{1}{\hat{\Phi}^{-1}(1/w)} \quad (3.4)$$

$$= w + \sum_{m \geq 2} a_m w^m, \quad |w| < 1, \quad (3.5)$$

is a biholomorphism of \mathbb{D}_1 onto $\bar{\mathbb{C}} \setminus M_c^{-1}$. It is not difficult to see that $\Phi^{-1}(w)$ is related to the Böttcher map ϕ_β by

$$\Phi(\beta) = \phi_\beta(\beta) = \lim_{n \rightarrow \infty} \sqrt[n]{Q_\beta^n(\beta)}.$$

Suppose $\beta \notin M_c^{-1}$ and $\Phi(\beta) = w \in \mathbb{D}_1$. By (1.4) and (2.2), the relation between β and ϵ is

$$\beta = \frac{4\epsilon^2}{2\epsilon - 1} \quad (\text{or } \epsilon = \frac{\beta \pm i\sqrt{4\beta - \beta^2}}{4}), \quad (3.6)$$

in particular, $\beta = -4\epsilon^2 + O(\epsilon^3)$ when ϵ is small. Thus, each β corresponds to two ϵ 's except when $\beta = \epsilon = 0$. (When $\beta = 4$ or equivalently $c = 1/4$, ϵ takes a unique value 1, but $4 \in M_c^{-1}$ or equivalently $1/4 \in M_c$, and $1 \in M_\mu^{-1}$.) As a result, each $w = \Phi(\beta)$ in \mathbb{D}_1 corresponds to two ϵ 's in $\bar{\mathbb{C}} \setminus M_\mu^{-1}$ except $w = \Psi(0) = 0$. By the Riemann Mapping Theorem, there exists a unique biholomorphic map

$$\Psi : \bar{\mathbb{C}} \setminus M_\mu^{-1} \rightarrow \mathbb{D}_1$$

satisfying $\Psi(0) = 0$ and $\Psi(\epsilon) = -2i\epsilon + O(\epsilon^2)$ when ϵ is small. Consequently, the following diagram commutes

$$\begin{array}{ccccc}
\epsilon \in \bar{\mathbb{C}} \setminus M_\mu^{-1} & \xrightarrow{\Psi} & \mathbb{D}_1 & \xrightarrow{\quad} & \bar{\mathbb{C}} \setminus M_\mu \ni \mu \\
(3.6) \downarrow & \searrow \Upsilon & \downarrow \Psi(\epsilon) \mapsto (\Psi(\epsilon))^2 & & \downarrow (1.4) \\
\beta \in \bar{\mathbb{C}} \setminus M_c^{-1} & \xrightarrow{\Phi} & \mathbb{D}_1 & \xrightarrow{\hat{\Phi}^{-1}(1/\cdot)} & \bar{\mathbb{C}} \setminus M_c \ni c.
\end{array}$$

In the diagram the map $\Upsilon : \bar{\mathbb{C}} \setminus M_\mu^{-1} \rightarrow \mathbb{D}_1$, $\epsilon \mapsto w$, is defined by

$$\Upsilon(\epsilon) = (\Psi(\epsilon))^2 = w.$$

When ϵ is small, $\Upsilon(\epsilon) = -4\epsilon^2 + O(\epsilon^3)$. Using $w = re^{i2\pi\theta}$, $0 \leq r < 1$, $0 \leq \theta < 1$, we specify the two branches Υ_\pm^{-1} of the inverse of Υ as the following:

$$\Upsilon_\pm^{-1}(re^{i2\pi\theta}) := \Psi^{-1}(\pm\sqrt{r}e^{i\pi\theta}). \quad (3.7)$$

On the other hand, Υ_\pm^{-1} can also be expressed in terms of Φ^{-1} . In view of relation (3.6), we can set

$$\Upsilon_\pm^{-1}(w) := \frac{\Phi^{-1}(w) \pm i\sqrt{\bar{r}}e^{i\pi\bar{\theta}}}{4}, \quad (3.8)$$

where $\bar{r} = |4\Phi^{-1}(w) - (\Phi^{-1}(w))^2|$ and $\bar{\theta} = \arg(4\Phi^{-1}(w) - (\Phi^{-1}(w))^2)$. It is easy to verify that the two inverses defined by (3.7) and (3.8) are consistent: When $w = re^{i2\pi\theta}$ with r small, we have $\bar{r} = 4r + O(r^2)$ and $\bar{\theta} = \theta + O(r^2)$. Hence, $(\Phi^{-1}(w) \pm i\sqrt{\bar{r}}e^{i\pi\bar{\theta}})/4 = \Psi^{-1}(\pm\sqrt{r}e^{i\pi\theta}) = \pm i\sqrt{r}e^{i\pi\theta}/2 + O(r)$.

Our integral curves for (3.3) are external rays of M_μ^{-1} , therefore, for fixed θ of even denominator, a curve γ of the form

$$\gamma : [0, 1) \rightarrow \bar{\mathbb{C}} \setminus M_\mu^{-1}, \quad r \mapsto \Upsilon^{-1}(re^{i2\pi\theta}),$$

with $\Upsilon^{-1}(w) = \Upsilon_-^{-1}(w)$ or $\Upsilon_+^{-1}(w)$ can serve as an integral curve along which the system (3.3) is integrated, from the anti-integrable limit $\gamma(0) = 0$ to $\gamma(1) \in \partial M_\mu^{-1}$.

THEOREM 3.2. *Suppose $0 \neq \hat{\epsilon} \notin M_\mu^{-1}$ and suppose $\{z_n\}_{n \geq 0}$, with $z_n = f_{1/\hat{\epsilon}}^n(z_0) \forall n \geq 0$, is a bounded orbit of the logistic map $f_{1/\hat{\epsilon}}$ with itinerary sequence $\{\alpha_n\}_{n \geq 0}$. Assume $z_n^*(\epsilon)$ is the solution of (3.3) integrated along an integral curve in $\bar{\mathbb{C}} \setminus M_\mu^{-1}$ connecting $\epsilon = 0$ to $\epsilon = \hat{\epsilon}$ subject to initial condition $z_n^*(0) = \alpha_n$ for every $n \geq 0$. Then the value of $z_n^*(\hat{\epsilon})$ is independent of integral curves, and $z_n^*(\hat{\epsilon}) = z_n$ for all n .*

Remark 3.3. There is another way to carry out the integration. Because of (3.8) we have

$$\frac{d}{d\epsilon} = \left(\frac{d\Upsilon_\pm^{-1}(w)}{dw} \right)^{-1} \frac{d}{dw}, \quad (3.9)$$

and the corresponding integral curves turn out to have the very simple form: $\{w \mid w = re^{i2\pi\theta}, 0 \leq r < 1, \theta \text{ fixed rational number}\}$.

Remark 3.4. Similar to [4] we can define the automorphism of the 2-shift induced by the monodromy constructed by traversing a closed curve which winds once around the Mandelbrot set M_μ in $\bar{\mathbb{C}} \setminus M_\mu$. Then the automorphism is an identity map, as can readily be seen from the theorem above. Indeed, in view of the commutative diagram above, M_μ is a degree two branched covering of M_c , with branch points at μ equal to 1 and ∞ , and M_μ^{-1} is a degree two branched covering of M_c^{-1} , with branch points at $\epsilon = 1$

and 0. Hence, a loop in $\mathbb{C} \setminus M_c$ corresponds only a “half” loop in $\mathbb{C} \setminus M_\mu$ joining the two roots of (1.4). Besides, it is easy to see that the two rays $\mathcal{R}(l(c)/2; K(q_c))$ and $\mathcal{R}((l(c)+1)/2; K(q_c))$ are interchanged correspondingly, and so are the two disjoint open sets V_0 and V_1 of the partition.

Remark 3.5. If $\{z_n\}$, $n \geq 0$, is a period- $(p+1)$ orbit of $f_{1/\epsilon}$ with itinerary $\{\overline{\alpha_0 \alpha_1 \dots \alpha_p}\}$, the solution in Theorem 3.2 satisfies $z_n^*(\epsilon) = z_{n+p+1}^*(\epsilon)$ for every $n \geq 0$. In this case, $z_n^*(\epsilon)$ can also be obtained by integrating a $(p+1)$ -coupled ODEs of the form

$$\frac{d}{d\epsilon} z_n = \left(1 - \epsilon^{p+1} \prod_{k=0}^p (1 - 2z_{n+k})^{-1} \right)^{-1} \sum_{N=0}^p \epsilon^N \left(\prod_{k=0}^N (1 - 2z_{n+k})^{-1} \right) z_{n+1+N} \quad (3.10)$$

starting from initial point $\epsilon = 0$ with periodicity $z_{n+1+p} = z_n$ and initial condition $z_n^*(0) = \alpha_n$ for every $0 \leq n \leq p$ (see [9]).

Theorem 3.2 together with Remark 3.5 provide an alternative method for finding all roots of a class of polynomials. Suppose we are interested in finding all periodic orbits of the map $z \mapsto \epsilon^{-1}z(1-z)$, say period-10, for instance. What we usually do is to solve a polynomial of 1024-degree for z_0 arising from the following algebraic relation:

$$\begin{aligned} z_1 &= \epsilon^{-1}z_0(1-z_0), \\ z_2 &= \epsilon^{-1}z_1(1-z_1), \\ &\vdots \\ z_p &= \epsilon^{-1}z_{p-1}(1-z_{p-1}), \\ z_0 &= \epsilon^{-1}z_p(1-z_p), \end{aligned} \quad (3.11)$$

with $p = 9$. If $0 \neq \epsilon \notin M_\mu^{-1}$, from Theorem 3.2 we know that the polynomial for z_0 has 1024 distinct roots, corresponding to 1024 distinct initial points for all of period-10 orbits (not all are of least period). Even if we have successfully find all roots of the polynomial, another question that concerns distinguishing the combinatorics of these roots is the itinerary of their corresponding orbits. In general, a root \tilde{z}_0 itself does not tell us this information. The following Corollary of Theorem 3.2 manifests how to find \tilde{z}_0 with any prescribed itinerary. (See Section 4.4 for an example of period-98.)

COROLLARY 3.6. *Let $0 \neq \hat{\epsilon} \notin M_\mu^{-1}$.*

- *The 2^{p+1} -degree polynomial arising from (3.11) for z_0 with $\epsilon = \hat{\epsilon}$ has 2^{p+1} distinct roots.*
- *Assume \tilde{z}_0 is one such root and the itinerary of its orbit is $\{\alpha_n\}_{n \geq 0}$. Then \tilde{z}_0 can be obtained by means of Theorem 3.2, namely $\tilde{z}_0 = z_0^*(\hat{\epsilon})$.*
- *\tilde{z}_0 can equivalently be obtained by integrating the $(p+1)$ -coupled ODEs (3.10).*

4. Visualization along external rays that terminate at Misiurewicz points. We use finitely many points that constitute an invariant subset to approximate the Julia set, consequently the infinitely coupled differential equations (3.3) become a finitely coupled ODEs. Then, we use the second order Runge-Kutta method to get numerical solutions of the ODEs.

For a specified initial condition $\{\alpha_n\}_{n \geq 0}$ in Theorem 3.2, it determines precisely one point $z_i^*(\hat{\epsilon})$ of the Julia set $J(f_{1/\hat{\epsilon}})$ for a given integer $i \geq 0$. Subsequently, for given i , a finite set of initial conditions $\{\alpha_{n,0}, \alpha_{n,1}, \dots, \alpha_{n,m}\}_{n \geq 0}$ give rise to a set of m number of points $\{z_{i,0}^*(\hat{\epsilon}), z_{i,1}^*(\hat{\epsilon}), \dots, z_{i,m}^*(\hat{\epsilon})\} \subset J(f_{1/\hat{\epsilon}})$. Suppose $\hat{\epsilon}$ is a Misiurewicz point, then in order to get a satisfactory geometric shape of the Julia set $J(f_{1/\hat{\epsilon}})$, we choose the set of our initial conditions for (3.3) in accordance with the critical orbit at that Misiurewicz point $\hat{\epsilon}$.

For $\theta \in \mathbb{R}/\mathbb{Z}$, define the two external rays $\mathcal{R}^+(\theta; M_\mu^{-1})$ and $\mathcal{R}^-(\theta; M_\mu^{-1})$ of angle θ of M_μ^{-1} by

$$\begin{aligned} \mathcal{R}^+(\theta; M_\mu^{-1}) &:= \{\Upsilon_+^{-1}(re^{-i2\pi\theta}) \mid 0 \leq r < 1\}, \\ \mathcal{R}^-(\theta; M_\mu^{-1}) &:= \{\Upsilon_-^{-1}(re^{-i2\pi\theta}) \mid 0 \leq r < 1\}. \end{aligned}$$

The angle θ of the just defined external rays is inherited from the angle of the external ray $\mathcal{R}(\theta; M_c)$ of the Mandelbrot set M_c . See the diagram in Section 3.

4.1. Angle 1/2. The landing point of the external ray $\mathcal{R}^+(1/2; M_\mu^{-1})$ (corresponding to the lines $\{\epsilon \mid 0 \leq \operatorname{Re}(\epsilon) < 0.25, \operatorname{Im}(\epsilon) = 0\}$ or $\{\mu \mid 4 < \operatorname{Re}(\mu), \operatorname{Im}(\mu) = 0\}$ or $\{c \mid \operatorname{Re}(c) < -2, \operatorname{Im}(c) = 0\}$) is a real number and equal to 0.25. The critical orbit for this Misiurewicz point takes the simple form $(1/2, 1, \bar{0})$. This suggests to consider the following initial conditions $\{z_0^*(0), z_1^*(0), \dots, z_m^*(0), 1, \bar{0}\}$ with $z_n^*(0) \in \{0, 1\}$ for all $0 \leq n \leq m$ in order to solve (3.3) numerically. With an initial condition of this kind, it follows that orbit points will converge to zero after $m + 2$ times iterations:

$$z_{m+1} = 1 \quad \text{and} \quad z_n = 0 \quad \forall n \geq m + 2.$$

Hence, (3.3) reduces to a system of $m + 1$ -coupled ODEs:

$$\frac{d}{d\epsilon} z_n = \sum_{N=0}^{m-n} \epsilon^N \left(\prod_{k=0}^N (1 - 2z_{n+k})^{-1} \right) z_{n+1+N}$$

with $0 \leq i \leq m$.

We set $m = 10$. Figures 4.1 (a)~(g) illustrate approximations of the Julia set $J(f_{1/\epsilon})$ by plotting the union of solutions $\bigcup_{i=0}^{12} z_i^*(\epsilon)$ for seven different values of ϵ integrated from $\epsilon = 0$ to $\epsilon = 0.25$ along the ray $\mathcal{R}^+(1/2; M_\mu^{-1})$. The seven values of ϵ are (a) 0, (b) 0.041666667, (c) 0.083333333, (d) 0.125, (e) 0.166666667, (f) 0.208333333, and (g) 0.25. Theoretically, each of Figures 4.1 (b)~(f) possesses 4096 points ($2^{12} = 4096$), whereas Figure 4.1 (g) consists of 2049 points ($2^{10} + \dots + 2^1 + 1 + 1 + 1 = 2049$).

4.2. Angle 1/6. It is known [6] that the critical orbit for the Misiurewicz point of angle 1/6 has the form $(1/2, f_{1/\epsilon}(1/2), f_{1/\epsilon}^2(1/2), f_{1/\epsilon}^3(1/2), f_{1/\epsilon}^4(1/2), \dots)$. With this in mind, we choose the following initial conditions $\{z_0^*(0), z_1^*(0), \dots, z_m^*(0), 1, \bar{10}\}$ with $z_n^*(0) \in \{0, 1\}$ for all $0 \leq n \leq m$ to deal with (3.3). The initial condition in this case indicates that, after $m + 2$ times iterations, orbits will become periodic with period 2. That is, $z_n = z_{n+2}$ for all $n \geq m + 2$. Hence, the orbit points z_n 's for $n \geq m + 2$ satisfy two coupled equations which read

$$\frac{d}{d\epsilon} z_n = \left(1 - \epsilon^2 \prod_{k=0}^1 (1 - 2z_{n+k})^{-1} \right)^{-1} \sum_{N=0}^1 \epsilon^N \left(\prod_{k=0}^N (1 - 2z_{n+k})^{-1} \right) z_{n+1+N}.$$

When $0 \leq n \leq m + 1$, orbit points z_n 's are governed by the following differential equations (see [9]):

$$\begin{aligned} \frac{d}{d\epsilon} z_n &= \sum_{N=0}^{m+1-n} \epsilon^N \left(\prod_{k=0}^N (1 - 2z_{n+k})^{-1} \right) z_{n+1+N} \\ &+ \left(1 - \epsilon^2 \prod_{k=0}^1 (1 - 2z_{m+2+k})^{-1} \right)^{-1} \sum_{N=0}^1 \epsilon^{m+2-n+N} \left(\prod_{k=0}^{m+2-n+N} (1 - 2z_{n+k})^{-1} \right) z_{m+3+N}. \end{aligned}$$

Hence, with the initial condition taken in this subsection, (3.3) reduces to a system of $(m + 4)$ -coupled ODEs.

We set $m = 12$. Figures 4.2 (a)~(g) display approximations of the Julia set $J(f_{1/\epsilon})$ by plotting the union of solutions $\bigcup_{n=0}^{15} z_n^*(\epsilon)$ for seven different values of ϵ integrated along the ray $\mathcal{R}^+(1/6; M_\mu^{-1})$. The seven values of ϵ are (a) 0, (b) $0.129889641 + 0.141065491i$, (c) $0.233392345 + 0.176828347i$, (d) $0.299652988 + 0.166937164i$, (e) $0.312689831 + 0.154912018i$, (f) $0.312597233 + 0.150118104i$, (g) $\frac{-i+i\sqrt{1-4i}}{4}$, (h) $\frac{-i+i\sqrt{1-4i}}{4}$, and (i) $\frac{-i+i\sqrt{1-4i}}{4}$. When $\epsilon = (-i + i\sqrt{1-4i})/4 \approx 0.312405267 + 0.150121295i$, the landing point of the ray $\mathcal{R}^+(1/6; M_\mu^{-1})$, Figures 4.2 (h) and (i) are also provided for

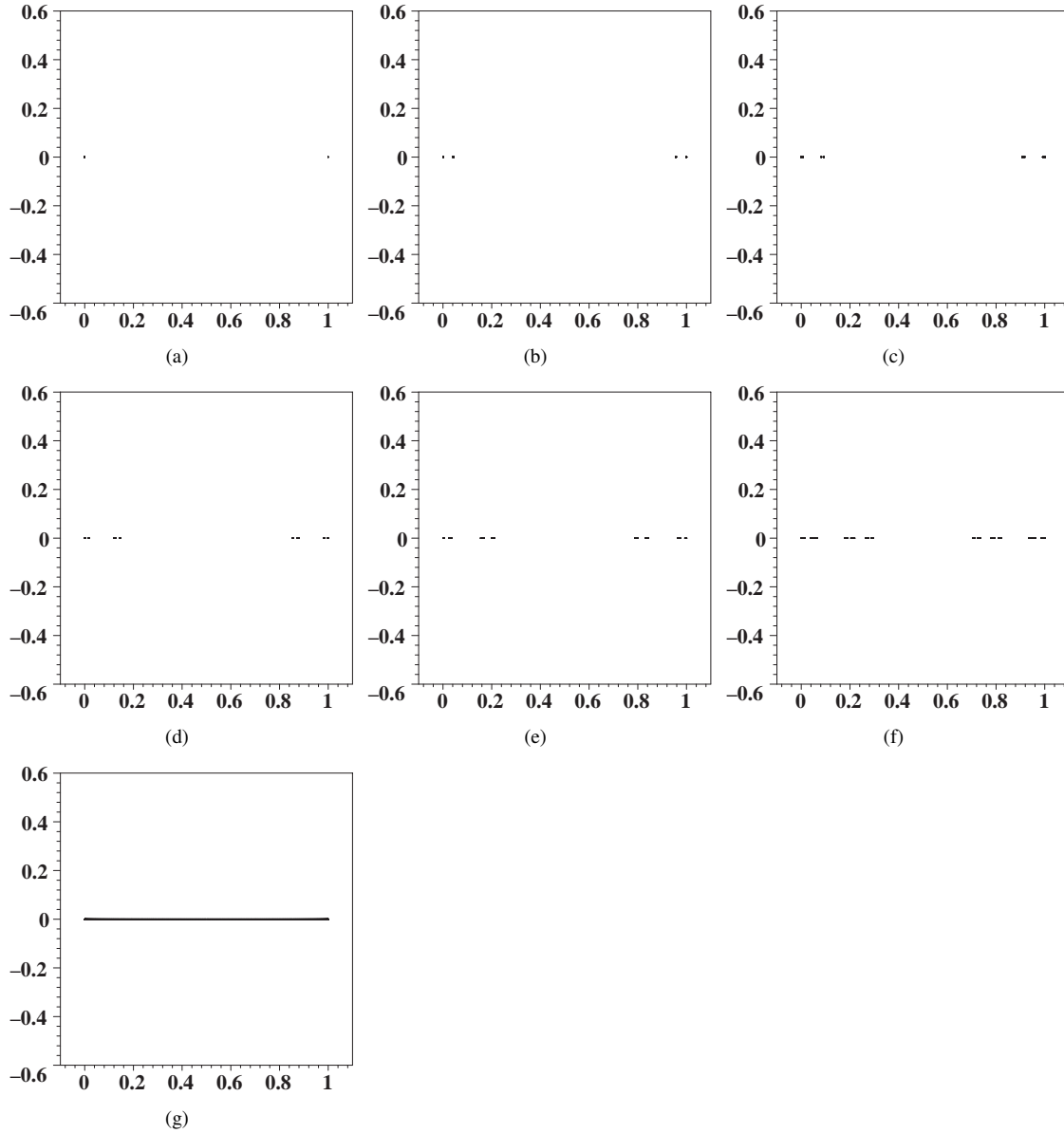


FIG. 4.1. The Julia set $J(f_{1/\epsilon})$ for seven different values of ϵ along $\mathcal{R}^+(1/2; M_\mu^{-1})$. See also the accompanying 3-D animation (2009AlongRealAxisRotate.mov [5.03MB]) for the numerical solution.

the sake of comparison. Figure 4.2 (h) shows the union of sets $f_{1/\epsilon}^{-12}(1/2), \dots, f_{1/\epsilon}^{-1}(1/2), 1/2, f_{1/\epsilon}(1/2), f_{1/\epsilon}^2(1/2),$ and $f_{1/\epsilon}^3(1/2)$, consisting of iterated preimages and images of the critical point $1/2$. Theoretically, Figures 4.2 (g) and (h) are identical. At this point, the picture of Julia set obtained by the OTIS programme (by means of the *distance estimate method* [27]) is shown in Figure 4.2 (i). Each of Figures 4.2 (b)~(f) possesses 16385 points ($2^{13} + \dots + 2^1 + 1 + 1 + 1 = 16385$), whereas each of Figures 4.2 (g) and (h) consists of 8194 points ($2^{12} + \dots + 2^1 + 1 + 1 + 1 + 1 = 8194$).

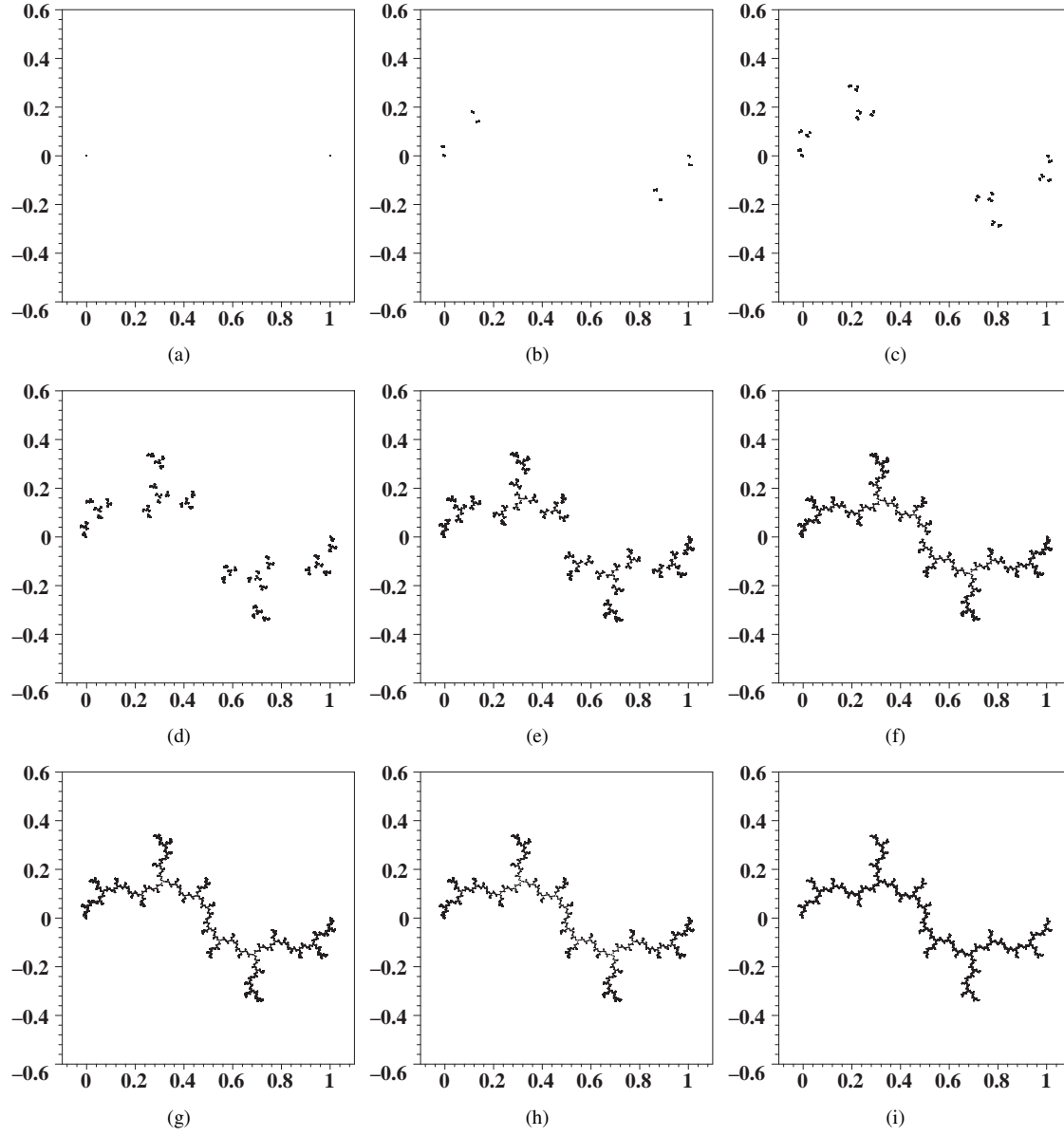


FIG. 4.2. The Julia set $J(f_{1/\epsilon})$ for seven different values of ϵ along $\mathcal{R}^+(1/6; M_\mu^{-1})$. See also the accompanying 3-D and 2-D animations (Exray1over6Rotate.mov [5.17MB] and Exray1over6Stars.mov [1.25MB]) for the numerical solutions.

4.3. Angle $5/12$. When the parameter is at the Misiurewicz point of angle $5/12$, the orbit of the critical point has the form $(1/2, f_{1/\epsilon}(1/2), f_{1/\epsilon}^2(1/2), f_{1/\epsilon}^3(1/2), f_{1/\epsilon}^4(1/2), \dots)$ (see [6]). Accordingly, we choose $\{z_0^*(0), z_1^*(0), \dots, z_m^*(0), 0, \bar{1}\}$ with $z_n^*(0) \in \{0, 1\}$ for all $0 \leq n \leq m$ to be the initial conditions for (3.3). As a result, orbit points will converge to the fixed point $1 - \epsilon$ after $m + 2$ times iterations, i.e. $z_n = z_{m+2} = 1 - \epsilon$ for all $n \geq m + 2$. Subsequently, (3.3) reduces to an $(m + 2)$ -coupled

ODEs:

$$\begin{aligned} \frac{d}{d\epsilon} z_n &= \sum_{N=0}^{m+1-n} \epsilon^N \left(\prod_{k=0}^N (1 - 2z_{n+k})^{-1} \right) z_{n+1+N} \\ &+ (1 - \epsilon(1 - 2z_{m+2})^{-1})^{-1} \epsilon^{m+2-n} \left(\prod_{k=0}^{m+2-n} (1 - 2z_{n+k})^{-1} \right) z_{m+3} \end{aligned}$$

for $0 \leq n \leq m + 1$.

We set $m = 14$. Figures 4.3 (a)~(g) approximate the Julia set $J(f_{1/\epsilon})$ by plotting the union of solutions $\bigcup_{n=0}^{16} z_n^*(\epsilon)$ for seven values of ϵ integrated along the ray $\mathcal{R}^+(5/12; M_\mu^{-1})$. The seven ϵ 's are (a) 0, (b) $0.126015870 + 0.027344314i$, (c) $0.225252678 + 0.031196957i$, (d) $0.266926087 + 0.010949307i$, (e) $0.271419899 + 0.002636994i$, (f) $0.271819409 + 0.000541256i$, (g) 0.271844506 , (h) 0.271844506 , and (i) 0.271844506 . The landing point of $\mathcal{R}^+(5/12; M_\mu^{-1})$ is a real number and is about $\epsilon \approx 0.271844506$. At this Misiurewicz point the non-zero fixed point is also real and is $1 - \epsilon \approx 0.728155494$. Figure 4.3 (h) shows the union of sets $f_{1/\epsilon}^{-15}(f_{1/\epsilon}^2(1/2)), \dots, f_{1/\epsilon}^{-2}(f_{1/\epsilon}^2(1/2)), f_{1/\epsilon}^{-1}(f_{1/\epsilon}^2(1/2)), f_{1/\epsilon}^2(1/2)$, and $f_{1/\epsilon}^3(1/2) = 1 - \epsilon$ for this Misiurewicz point. Theoretically, Figures 4.3 (g) and (h) are identical. At this point, the picture of Julia set obtained by the OTIS programme is provided in Figure 4.3 (i) for the sake of comparison. Each figure (b)~(f) possesses 65536 distinct points ($2^{15} + 2^{14} + \dots + 2 + 1 + 1 = 65536$), whereas each of (g) and (h) consists of 49153 distinct points ($3 \cdot 2^{13} + \dots + 3 \cdot 2^1 + 3 + 2 + 1 + 1 = 49153$).

4.4. Angle 1/128. When the parameter ϵ is located at one of the Misiurewicz points of angle 1/128 (for example, $\epsilon \approx 0.567999678 + 0.348835133i$), it appears that at least up to $m = 50$ the preimage set $\bigcup_{n=0}^m f_{1/\epsilon}^{-n}(z)$ for z being the either fixed point of the map $f_{1/\epsilon}$ does not generate satisfactory picture of the Julia set. The preimage set apparently does not agree with the one generated by using the distance estimate method. And to the best knowledge of ours, we do not aware of any z that would do so. Hence, instead of attempting to draw the picture of the Julia set, we employ (3.3) to obtain periodic orbits.

We choose our initial condition for (3.10) to be

$$\begin{aligned} \{z_0^*(0), z_1^*(0), \dots, z_{97}^*(0)\} &= \\ &\{0, 1, 0, 0, 0, 1, 1, 0, 1, 1, 0, 0, 0, 0, 0, 1, 0, 1, 0, 0, 1, 1, 1, 0, 0, 1, 0, 1, 1, 1, \\ &0, 1, 1, 1, 0, 0, 0, 0, 0, 0, 1, 0, 0, 1, 0, 0, 0, 1, 1, 0, 1, 0, 0, 0, 1, 0, 1, 0, 1, \\ &1, 0, 0, 1, 1, 1, 1, 0, 0, 0, 1, 0, 0, 1, 1, 0, 1, 0, 1, 1, 1, 1, 0, 0, 1, 1, 0, 1, \\ &1, 1, 1, 0, 1, 1, 1, 1\}. \end{aligned} \quad (4.1)$$

Figure 4.4 (a) depicts the union of the solution $\bigcup_{n=0}^{97} z_n^*(\epsilon)$ for $\epsilon = 0.567999678 + 0.348835133i$ integrated along the ray $\mathcal{R}^+(1/128; M_\mu^{-1})$. (It took 57 minutes for us to get the solution.) In the figure, the set in yellow color is comprised of the Julia set $J(f_{1/\epsilon})$ and the dynamic rays of angles 1/256 and 129/256. The two dynamic rays, which terminate at the real number 1/2, divide the complex plane into two disjoint regions. The 98 black points represent the 98-period solution $z_0 \mapsto z_1 \mapsto \dots \mapsto z_{97} \mapsto z_0$ with itinerary sequence listed in (4.1). The line segments in cyan color connecting points z_i to z_{i+1} show how these periodic points are mapped to the next ones.

As is clear from Table 4.1, which shows the numerical error for the obtained period-98 orbit, the result is rather satisfactory.

Remark 4.1. The numerical computation in this section suggests that $z_n^*(\epsilon)$ for every $n \geq 0$ converges to a point in $J(f_{1/\epsilon})$ as ϵ approaches a Misiurewicz point along the parameter ray. This will be the issue considered in a paper in preparation.

5. Algorithms for determining the parameter rays $\mathcal{R}(\theta; M_c)$.

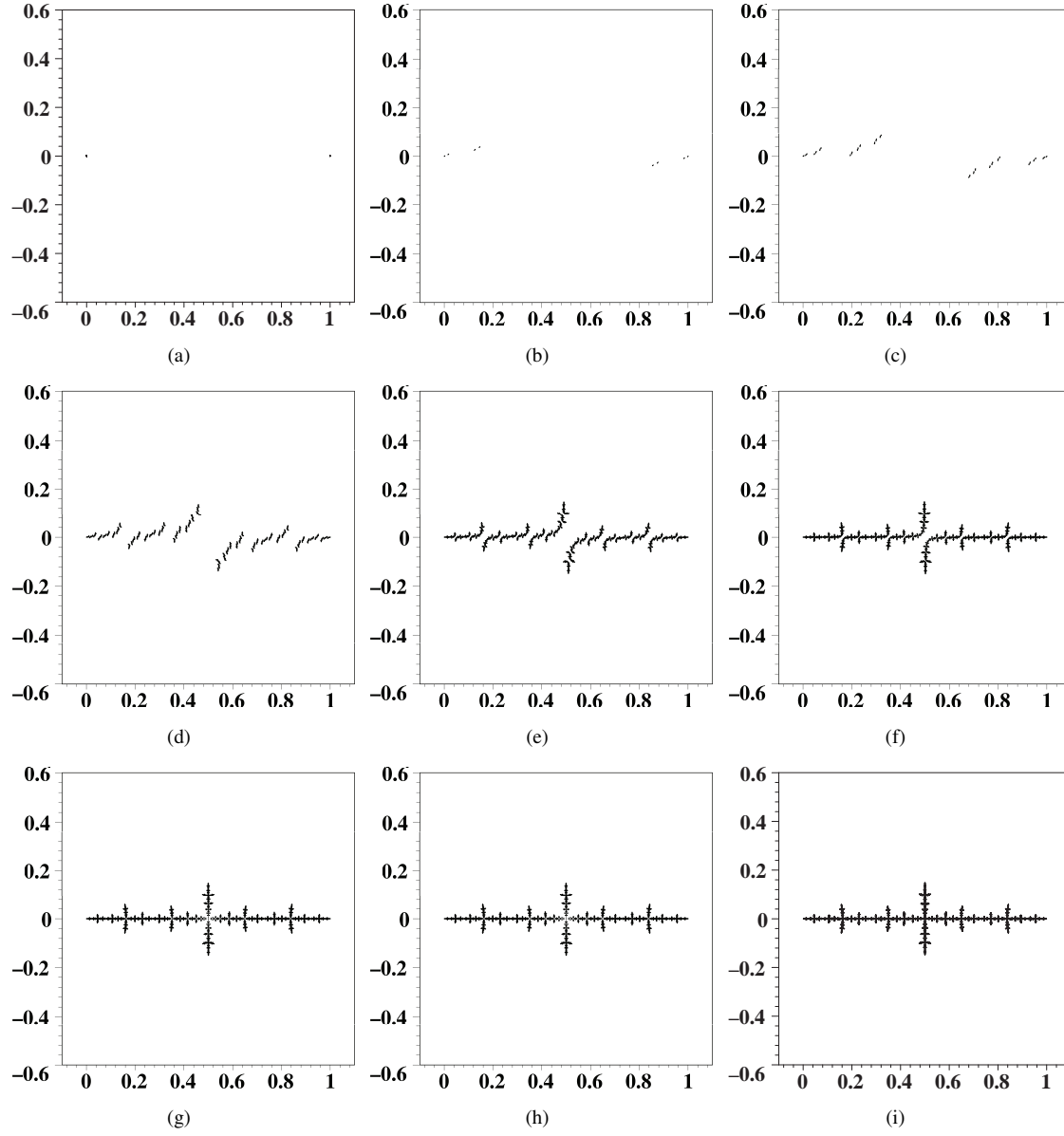


FIG. 4.3. The Julia set $J(f_{1/\epsilon})$ for seven different ϵ 's along $\mathcal{R}^+(5/12; M_\mu^{-1})$. See also the accompanying 3-D and 2-D animations (Exray5over12Rotate.mov [21.8MB] and Exray5over12Stars.mov [1.33MB]) for the numerical solutions.

5.1. Jungreis-Ewing-Schober (JES) algorithm (series expansion). One can expand $\hat{\Phi}^{-1}(w)$ as

$$\hat{\Phi}^{-1}(w) = w + \sum_{m \geq 0} b_m w^{-m}, \quad |w| > 1. \quad (5.1)$$

When w is near the infinity, one has [2, 16, 20]

$$\begin{aligned} \hat{\Phi}^{-1}(w) &= \hat{\Phi}_n^{-1}(w) + O(w^{2-2^{n+1}}), \\ \hat{\Phi}_{n+1}^{-1}(w) &= \hat{\Phi}_n^{-1}(w) + O(w^{2-2^{n+1}}). \end{aligned}$$

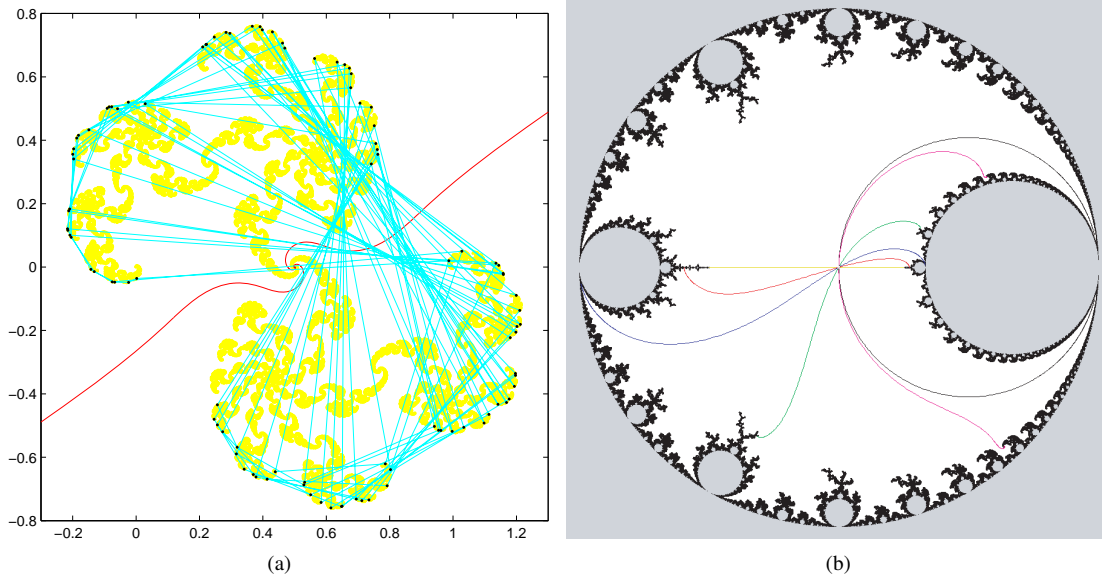


FIG. 4.4. (a) The Julia set, the dynamic rays of angles $1/256$ and $129/256$, and a 98-Period solution. (b) Parameter rays of angles 0 (black), $1/2$ (yellow), $1/3$ (blue), $1/6$ (green), $5/12$ (red) and $1/128$ (magenta) in the complement of the “inside-out” Mandelbrot set M_μ^{-1} .

These results point out that the convergence $\hat{\Phi}_n^{-1} \rightarrow \hat{\Phi}^{-1}$ is remarkably rapid. From (2.7) evidently one has

$$q_{\hat{\Phi}_n^{-1}(w)}^n(\hat{\Phi}_n^{-1}(w)) = w^{2^n}, \quad (5.2)$$

thus one also has

$$\begin{aligned} q_{\hat{\Phi}_n^{-1}(w)}^n(\hat{\Phi}^{-1}(w)) &= \hat{\Phi}^{-1}(w)^{2^n} + 2^{n-1}\hat{\Phi}^{-1}(w)^{2^{n-1}} + \dots \\ &= w^{2^n} + O(w^{1-2^n}). \end{aligned}$$

In order to calculate the coefficients b_m , Ewing and Schober [18] further employed the following expansion

$$q_{\hat{\Phi}_n^{-1}(w)}^n(\hat{\Phi}^{-1}(w)) = \sum_{m \geq 0} \Gamma_{n,m} w^{2^n - m}, \quad |w| > 1,$$

and showed that

- $\Gamma_{n,0} = 1$ for $n \geq 0$,
- $\Gamma_{n,m} = 0$ for $n \geq 1$ and $1 \leq m \leq 2^{n+1} - 2$,
- $\Gamma_{0,m} = b_{m-1}$ for $m \geq 1$.

Moreover, they obtained the following very useful backward recursion formula

$$\Gamma_{n,m} = \frac{1}{2} \left(\Gamma_{n+1,m} - \Gamma_{0,m-2^{n+1}+1} - \sum_{k=2^{n+1}-1}^{m-2^{n+1}+1} \Gamma_{n,k} \Gamma_{n,m-k} \right), \quad (5.3)$$

TABLE 4.1

Error verification of the obtained period-98 orbit. In the table $Error_n = |z_{n+1} - \epsilon^{-1}z_n(1 - z_n)|$.

n	z_n	$Error_n$	n	z_n	$Error_n$
0	0.2219225 + 0.7025727 <i>i</i>	6.3875180E-05	49	1.1966416 - 0.3356524 <i>i</i>	5.3086075E-05
1	1.1585066 - 0.0235395 <i>i</i>	1.4414667E-05	50	0.2103574 + 0.6941909 <i>i</i>	6.4301186E-05
2	-0.2097154 + 0.1833763 <i>i</i>	2.8986387E-05	51	1.1440918 + 0.0053744 <i>i</i>	1.2972271E-05
3	-0.0769903 + 0.5055563 <i>i</i>	6.4765670E-05	52	-0.2161586 + 0.1205603 <i>i</i>	2.6179199E-05
4	0.6787778 + 0.6103129 <i>i</i>	3.8167939E-05	53	-0.1819294 + 0.4157538 <i>i</i>	5.8981657E-05
5	0.5836139 - 0.7425738 <i>i</i>	5.3941587E-05	54	0.3912507 + 0.7580534 <i>i</i>	5.8182569E-05
6	1.1130641 - 0.4649153 <i>i</i>	6.2775251E-05	55	1.1685276 - 0.4273271 <i>i</i>	5.8966289E-05
7	0.5629855 + 0.6579069 <i>i</i>	3.8906294E-05	56	0.4302632 + 0.7417198 <i>i</i>	5.3263175E-05
8	0.8028143 - 0.6389108 <i>i</i>	6.2640044E-05	57	1.0978909 - 0.4920903 <i>i</i>	6.4197221E-05
9	1.0279777 + 0.0499355 <i>i</i>	3.9182835E-06	58	0.6341584 + 0.6465697 <i>i</i>	4.0244363E-05
10	-0.0749811 - 0.0467890 <i>i</i>	6.8983769E-06	59	0.6948383 - 0.7321181 <i>i</i>	6.0425768E-05
11	-0.1424939 - 0.0072215 <i>i</i>	1.2897096E-05	60	1.1802352 - 0.2225318 <i>i</i>	2.6466541E-05
12	-0.2153507 + 0.1159154 <i>i</i>	2.6035531E-05	61	0.0290513 + 0.5151846 <i>i</i>	5.9220737E-05
13	-0.1872256 + 0.4069632 <i>i</i>	5.8673982E-05	62	0.7563540 + 0.3898687 <i>i</i>	2.5085521E-05
14	0.3667061 + 0.7596082 <i>i</i>	5.9770305E-05	63	0.2729780 - 0.5195723 <i>i</i>	3.0329039E-05
15	1.1934887 - 0.3764129 <i>i</i>	5.5542720E-05	64	0.4136317 - 0.6693413 <i>i</i>	4.0814691E-05
16	0.2957900 + 0.7375319 <i>i</i>	6.1304841E-05	65	0.7920460 - 0.6899405 <i>i</i>	6.4270209E-05
17	1.1981355 - 0.2054721 <i>i</i>	2.8469686E-05	66	1.1354542 + 0.0121828 <i>i</i>	1.2292203E-05
18	-0.0242742 + 0.5200233 <i>i</i>	6.3262148E-05	67	-0.2085970 + 0.1008453 <i>i</i>	2.4749552E-05
19	0.7420300 + 0.5043344 <i>i</i>	3.1391820E-05	68	-0.1971045 + 0.3726714 <i>i</i>	5.5677737E-05
20	0.3782347 - 0.6620753 <i>i</i>	4.1770666E-05	69	0.2838202 + 0.7404911 <i>i</i>	6.2588372E-05
21	0.7344504 - 0.7348769 <i>i</i>	6.3818769E-05	70	1.2121601 - 0.1807470 <i>i</i>	2.9190269E-05
22	1.2102211 - 0.1365538 <i>i</i>	2.5666153E-05	71	-0.0848946 + 0.5053958 <i>i</i>	6.5242058E-05
23	-0.1491321 + 0.4330886 <i>i</i>	5.7710326E-05	72	0.6729565 + 0.6276282 <i>i</i>	4.0514142E-05
24	0.4621315 + 0.7061330 <i>i</i>	4.7823637E-05	73	0.6145108 - 0.7595809 <i>i</i>	5.8821381E-05
25	0.9971740 - 0.5182167 <i>i</i>	6.1895721E-05	74	1.1769789 - 0.4165227 <i>i</i>	5.8631822E-05
26	0.7514826 + 0.4457438 <i>i</i>	2.8202094E-05	75	0.3982546 + 0.7483376 <i>i</i>	5.7346698E-05
27	0.3167554 - 0.5892330 <i>i</i>	3.5711366E-05	76	1.1418124 - 0.4330971 <i>i</i>	5.6980690E-05
28	0.5510044 - 0.7185475 <i>i</i>	4.9312520E-05	77	0.4692519 + 0.6906166 <i>i</i>	4.6614772E-05
29	1.0338513 - 0.5058499 <i>i</i>	6.2352731E-05	78	0.9614469 - 0.5156618 <i>i</i>	5.8903453E-05
30	0.7064254 + 0.5170933 <i>i</i>	2.8064090E-05	79	0.7609685 + 0.3705734 <i>i</i>	2.6060172E-05
31	0.4393642 - 0.6456632 <i>i</i>	3.8444416E-05	80	0.2562487 - 0.4979062 <i>i</i>	3.1130695E-05
32	0.7863752 - 0.6207580 <i>i</i>	6.1844916E-05	81	0.3700267 - 0.6545749 <i>i</i>	4.1230461E-05
33	0.9864725 + 0.0201376 <i>i</i>	1.3008316E-06	82	0.7121826 - 0.7369043 <i>i</i>	6.2316089E-05
34	0.0021955 - 0.0358438 <i>i</i>	2.1681250E-06	83	1.2017319 - 0.1874451 <i>i</i>	2.8353210E-05
35	-0.0235755 - 0.0483518 <i>i</i>	3.6743668E-06	84	-0.0584713 + 0.4990813 <i>i</i>	6.3430289E-05
36	-0.0676149 - 0.0476191 <i>i</i>	6.4670736E-06	85	0.6769645 + 0.5657264 <i>i</i>	3.3567951E-05
37	-0.1318322 - 0.0142150 <i>i</i>	1.2083946E-05	86	0.5315292 - 0.6789118 <i>i</i>	4.6744796E-05
38	-0.2046071 + 0.0940290 <i>i</i>	2.4355368E-05	87	0.9411586 - 0.5026027 <i>i</i>	5.6971729E-05
39	-0.1997678 + 0.3559783 <i>i</i>	5.4860336E-05	88	0.7419056 + 0.3251555 <i>i</i>	2.3055403E-05
40	0.2467300 + 0.7256318 <i>i</i>	6.4517541E-05	89	0.2564449 - 0.4344726 <i>i</i>	2.6517874E-05
41	1.1992639 - 0.0893727 <i>i</i>	2.3756693E-05	90	0.3189469 - 0.5684711 <i>i</i>	3.3580652E-05
42	-0.1971714 + 0.3411496 <i>i</i>	5.3447602E-05	91	0.5292255 - 0.6873913 <i>i</i>	4.6425232E-05
43	0.2204670 + 0.7021034 <i>i</i>	6.3964363E-05	92	0.9540823 - 0.5151739 <i>i</i>	5.8339503E-05
44	1.1580259 - 0.0201055 <i>i</i>	1.4481666E-05	93	0.7626346 + 0.3553978 <i>i</i>	2.6407905E-05
45	-0.2126643 + 0.1771905 <i>i</i>	2.9142347E-05	94	0.2463359 - 0.4799620 <i>i</i>	3.1157386E-05
46	-0.0912774 + 0.5007116 <i>i</i>	6.5087707E-05	95	0.3406883 - 0.6379125 <i>i</i>	4.0787600E-05
47	0.6580502 + 0.6383887 <i>i</i>	4.0768346E-05	96	0.6478187 - 0.7556505 <i>i</i>	6.0213525E-05
48	0.6502528 - 0.7545769 <i>i</i>	6.0267661E-05	97	1.1970073 - 0.3417854 <i>i</i>	5.3460189E-05

which determines coefficient $\Gamma_{n,m}$ for $n \geq 0$ and $m \geq 2^{n+1} - 1$ in terms of $\Gamma_{j,k}$ with $j \geq n + 1$ and $k \leq m$. According to [2, 18, 20], all $\Gamma_{n,m}$ are real numbers, and all b_m are dyadic rationals. Some calculations by hand using (5.3) show that the first six coefficients are $b_0 = -1/2$, $b_1 = 1/8$, $b_2 = -1/4$, $b_3 = 15/128$, $b_4 = 0$, and $b_5 = -47/1024$. The recursion formula (5.3) can serve as an algorithm and can be programmed very easily and effectively by computer.

Having found the coefficients b_m of the Laurent series for $\hat{\Phi}^{-1}$, the coefficients a_m of the Taylor

series (3.5) for Φ^{-1} can be determined by (3.4) to be [17]

$$a_m = -b_{m-2} - \sum_{j=2}^{m-1} a_j b_{m-1-j}.$$

Some coefficients are $a_2 = 1/2$, $a_3 = 1/8$, $a_4 = 1/4$, $a_5 = 15/128$, $a_6 = 0$, and $a_7 = 81/1024$.

5.2. OTIS algorithm (Newton's method). In this subsection we explain the algorithm used in the OTIS programme to draw the parameter rays $\mathcal{R}(\theta; M_c)$ with an error estimate. Newton's method is the main tool. (Remark: One of the authors learned its principle by M. Shishikura, but this idea of using Newton's method is probably well-known for many other people working on complex dynamics.) More precisely, the algorithm gives finitely many points that enough approximate the set $\mathcal{R}(\theta; M_c)$ within a given precision.

5.2.1. The algorithm: theoretical settings. We first consider an algorithm to calculate $c \in \mathcal{R}(\theta; M_c)$ with

$$c = \hat{\Phi}^{-1}(re^{2\pi i\theta}) \iff \hat{\Phi}(c) = \hat{\phi}_c(c) = re^{2\pi i\theta}$$

for given $\theta \in \mathbb{R}/\mathbb{Z}$ and $r > 1$. By (2.4), we have

$$\hat{\phi}_c(q_c^n(c)) = (re^{2\pi i\theta})^{2^n} = r^{2^n} e^{2\pi i \cdot 2^n \theta}$$

for any $n \in \mathbb{N}$. Now we assume that n is very large and $q_c^n(c)$ is enough close to infinity. Since we have $\hat{\phi}_c(z)/z \rightarrow 1$ as $z \rightarrow \infty$ by (2.5), we have a "rough" approximation

$$q_c^n(c) \approx \hat{\phi}_c(q_c^n(c)) = r^{2^n} e^{2\pi i \cdot 2^n \theta} =: t.$$

Now our task is to solve the equation $q_c^n(c) = t$. (In Theorem 5.1 we shall give an error estimate of the root caused by this approximation.)

A bit more generally, for given $n \in \mathbb{N}$ and $t \in \mathbb{C}$, we want to solve the equation

$$\mathcal{P}_n(c) := q_c^n(c) - t = 0$$

numerically. Now $\mathcal{P}_n(c)$ is a polynomial of degree 2^n in variable c . When n is large, it is not possible to find the roots algebraically. For this kind of problem, a method which is commonly used is *Newton's method* (see [19] for example). It is given as follows:

Newton's method. Let F be a polynomial of degree more than one. We say the function

$$N(w) = N_F(w) := w - \frac{F(w)}{F'(w)}$$

is the *Newton map* of F . If $F(\alpha) = 0$ and w_0 is sufficiently close to α , then $N^k(w_0) \rightarrow \alpha$ as $k \rightarrow \infty$ at least exponentially fast. (More precisely, there exist constants $C > 0$ and $0 < \lambda < 1$ such that $|w_k - \alpha| \leq C\lambda^k$. When α is a simple root of F , we have $|w_k - \alpha| = O(|w_{k-1} - \alpha|^2)$. In this case the convergence is super-exponentially fast.)

Now we apply this method to $F = \mathcal{P}_n$ in variable c instead of w . In this case the Newton map is

$$N(c) = N_{n,t}(c) := c - \frac{\mathcal{P}_n(c)}{\mathcal{P}'_n(c)}$$

where $\mathcal{P}'_n(c) := \frac{d\mathcal{P}_n}{dc}(c)$, a polynomial of degree $2^n - 1$. If the initial value c_0 is sufficiently close to a zero of $\mathcal{P}_n(c)$, the sequence

$$c_0 \xrightarrow{N} N(c_0) \xrightarrow{N} N^2(c_0) \xrightarrow{N} N^3(c_0) \xrightarrow{N} \dots$$

converges to a zero of $\mathcal{P}_n(c)$.

To proceed the iteration numerically, we need to calculate $\mathcal{P}_n(c)$ and $\mathcal{P}'_n(c)$ with given c . The calculation of $\mathcal{P}_n(c) = q_c^n(c) - t$ is essentially the same as iteration of $q_c(z) = z^2 + c$. How about $\mathcal{P}'_n(c)$?

Let ' denote $\frac{d}{dc}$. Then we have

$$\begin{aligned} \mathcal{P}'_n(c) &= (q_c^n(c))' \\ &= ((q_c^{n-1}(c))^2 + c)' \\ &= 2(q_c^{n-1}(c))' q_c^{n-1}(c) + 1 \\ &= 2\mathcal{P}'_{n-1}(c) q_c^{n-1}(c) + 1. \end{aligned}$$

It follows that if we set $C_k := q_c^k(c)$ and $D_k := (q_c^k(c))'$ for each $1 \leq k \leq n$, the recursive formulae

$$\begin{cases} C_1 = c, & C_k = C_{k-1}^2 + c \\ D_1 = 1, & D_k = 2D_{k-1}C_{k-1} + 1 \end{cases}$$

will give the values of $\mathcal{P}_n(c) = C_n - t$ and $\mathcal{P}'_n(c) = D_n$ respectively. Hence the Newton map can be written as

$$N : c \mapsto c - \frac{C_n - t}{D_n}.$$

5.2.2. The algorithm: practical settings. For fixed $R > 1$, called the *maximal radius*, and a fixed integer D , consider the subset

$$\mathcal{R} := \left\{ \hat{\Phi}^{-1}(re^{2\pi i\theta}) : R^{1/2^D} \leq r < R \right\}$$

of the parameter ray $\mathcal{R}(\theta; M_c)$. If R is sufficiently large, \mathcal{R} reaches enough close to ∞ . If D is sufficiently large, $R^{1/2^D}$ is close to 1 and this implies that \mathcal{R} reaches enough close to (the boundary of) M_c . Hence we call D the *depth* of \mathcal{R} . Let us try to approximate this set \mathcal{R} by finitely many points. (We always draw a bounded domain with a finite number of pixels. Hence drawing the subset \mathcal{R} is reasonable.)

For any r with $R^{1/2^D} \leq r \leq R$, one can approximate $c = \hat{\Phi}^{-1}(re^{2\pi i\theta})$ by means of Newton's method under a suitable choice of the initial value. (We call this r the *radial parameter*.) Let us fix an integer $S > 0$ and call it the *sharpness*. We will pick up SD radial parameters $\{r_m\}_{m=1}^{SD}$ and calculate (approximate) SD points $\{c_m\}_{m=1}^{SD}$ on \mathcal{R} . Then we will join the sequence c_m by segments in the computer display. This is what we mean by "drawing \mathcal{R} ".

First we divide the interval $[R^{1/2^D}, R)$ into D sub-intervals

$$[R^{1/2^D}, R^{1/2^{D-1}}), [R^{1/2^{D-1}}, R^{1/2^{D-2}}), \dots, [R^{1/2^2}, R^{1/2}), [R^{1/2}, R),$$

and we pick up S radial parameters from each sub-intervals as follows: For each $k = 1, 2, \dots, D$, we define S radial parameters

$$R^{1/2^k}, R^{1/2^{k-1+(S-1)/S}}, \dots, R^{1/2^{k-1+1/S}}$$

contained in the sub-interval $[R^{1/2^k}, R^{1/2^{k-1}}]$. (The boundary of M_c is very complicated so it would be reasonable to choose r 's in this way.) We enumerate these radial parameters as follows:

$$\begin{cases} m := (k-1)S + j & (1 \leq j \leq S), \\ r_m := R^{1/2^{m/S}} = R^{1/2^{k-1+j/S}}. \end{cases}$$

Note that we have $r_1 > r_2 > \dots > r_{SD}$. (This enumeration by m would be used only when we plot the segments. When we apply Newton's method to approximate c_m , we use loops by k and j .) Now we are ready to apply Newton's method to calculate $\left\{ c_m = \hat{\Phi}^{-1}(r_m e^{2\pi i \theta}) \right\}_{m=1}^{SD}$.

When $r_m \in [R^{1/2^k}, R^{1/2^{k-1}}]$, we have $r_m^{2^k} \in [R, R^2]$ thus the value

$$\hat{\phi}_{c_m}(q_{c_m}^k(c_m)) = r_m^{2^k} e^{2\pi i \theta \cdot 2^k} := t_m$$

satisfies $|t_m| \geq R$. Hence if R is sufficiently large, we have

$$t_m = \hat{\phi}_{c_m}(q_{c_m}^k(c_m)) \approx q_{c_m}^k(c_m).$$

Under a suitable choice of the initial value $c_{m,0}$, its orbit by the Newton map N_{k,t_m} will give an approximation of c_m with $q_{c_m}^k(c_m) = t_m$. More precisely, we choose $c_{m,0}$ as follows:

- Since R is enough large, we have $\hat{\Phi}^{-1}(Re^{2\pi i \theta}) \approx Re^{2\pi i \theta}$ (since $\hat{\Phi}(c)/c \rightarrow 1$ as $c \rightarrow \infty$.) We set this value $c_0 := Re^{2\pi i \theta}$. (*Remark:* This part can be improved by using the expansion $\hat{\Phi}^{-1}(w) = w - 1/2 + 1/(8w) + \dots$ (namely (5.1)).)
- By using the initial value $c_0 = c_{1,0}$, we iterate the Newton map N_{1,t_1} sufficiently many times, say L_1 times. Set c_1 as its result. That is.

$$c_1 := N_{1,t_1}^{L_1}(c_0).$$

- Inductively, for any $1 \leq m \leq DS$ with $m = (k-1)S + j$, $1 \leq j \leq S$, we use c_{m-1} as the initial value $c_{m,0}$ and set

$$c_m := N_{k,t_m}^{L_m}(c_{m-1})$$

with sufficiently large integer L_m . The value c_{m-1} is presumably a "neighbor" of c_m on \mathcal{R} so it is the best possible initial value for Newton's method. We should enlarge L_m when D is large, because better precision would be required when c_m is close to M_c .

Finally join the set $\{c_m : 1 \leq m \leq DS\}$ by segments. This will give an approximation of \mathcal{R} .

5.2.3. Error estimate. In this algorithm we solve the equation $q_c^n(c) = t$ instead of solving $\hat{\phi}_c(q_c^n(c)) = t$ for given $t \in \mathbb{C}$. Let us establish an error estimate by this approximation.

Let \mathbb{D}_r denote the set $\{z \in \mathbb{C} : |z| < r\}$. It is well-known that $M_c \subset \overline{\mathbb{D}}_2$. Hence we fix any $r > 2$ so that \mathbb{D}_r is a neighborhood of M_c . Now we assume that $|c| \leq r$. Then we have:

THEOREM 5.1. *Let us fix t with sufficiently large modulus $|t| = R \gg 0$. Let c be a root of $q_c^n(c) = t$. Then there exists a solution \hat{c} of $\hat{\phi}_{\hat{c}}(q_{\hat{c}}^n(\hat{c})) = t$ such that*

$$|\hat{c} - c| = O\left(\frac{1}{2^n R^{2-1/2^n} (R^{1/2^n} - 1)}\right).$$

When $n > \log_2 \log R$, we have a uniform estimate

$$|\hat{c} - c| = O\left(\frac{1}{R^2 \log R}\right).$$

Here “sufficiently large R ” means that r/R is sufficiently small. This theorem implies that we would have better approximation of the parameter rays when R is large. However, note that this estimate does not count the rounding errors coming from Newton’s method.

Proof. The equation $\hat{\phi}_c(q_c^n(c)) = t$ is equivalent to $q_c^n(c) = \hat{\phi}_c^{-1}(t)$. Let us start with some calculations on $\hat{\phi}_c^{-1}$.

LEMMA 5.2. *For any $c \in \mathbb{C}$, the map $\hat{\phi}_c$ has the expansion near ∞ as follows:*

$$t = \hat{\phi}_c(z) = z + \frac{c}{2z} - \frac{c(c-2)}{z^3} + O\left(\frac{1}{z^5}\right).$$

Moreover, we have

$$z = \hat{\phi}_c^{-1}(t) = t - \frac{c}{2t} + \frac{c(3c-8)}{4t^3} + O\left(\frac{1}{t^5}\right).$$

Proof. We give a sketch of the proof. Recall the fact that $\hat{\phi}_c(z) = \lim_{n \rightarrow \infty} (q_c^n(z))^{1/2^n}$, where $(z^{2^n} + \dots)^{1/2^n} = z + O(1)$ (see (2.3)). Let $\hat{\phi}_n(z) = (q_c^n(z))^{1/2^n}$, then it is not difficult to check $\hat{\phi}_{n+1}(z) - \hat{\phi}_n(z) = O(1/z^{2^{n+1}-1})$, and this implies that

$$\hat{\phi}_c(z) = \hat{\phi}_n(z) + O(1/z^{2^{n+1}-1}).$$

Now we have the expansion of $\hat{\phi}_c$ above by an explicit calculation of $\hat{\phi}_n(z)$. The expansion of $\hat{\phi}_c^{-1}$ follows by using $z = t - c/2z + \dots$. \square

By this lemma we have

$$\left| (q_c^n(c) - t) - (q_c^n(c) - \hat{\phi}_c^{-1}(t)) \right| \leq \left| -\frac{c}{2t} + O\left(\frac{1}{t^3}\right) \right| \leq \frac{M}{R}.$$

for some constant $M > 0$ independent of $|c| \leq r$ and $R = |t| \gg 0$.

Now suppose that c is a root of $q_c^n(c) - t = 0$. We want to apply Rouché’s theorem, so that there exists \hat{c} near c such that $q_{\hat{c}}^n(\hat{c}) - \hat{\phi}_{\hat{c}}^{-1}(t) = 0$. It is enough to show that there exists a circle $\{\hat{c} \in \mathbb{C} : |\hat{c} - c| = \rho\}$ with $\rho > 0$ given as in the estimates in the statement such that

$$|q_{\hat{c}}^n(\hat{c}) - t| = |q_{\hat{c}}^n(\hat{c}) - q_c^n(c)| > \frac{M}{R}$$

for all \hat{c} on the circle. Let us consider the local behavior of the map $\hat{c} \mapsto q_{\hat{c}}^n(\hat{c})$ about c . Since we have

$$q_{\hat{c}}^n(\hat{c}) - q_c^n(c) = (q_c^n(c))'(\hat{c} - c) + O(|\hat{c} - c|^2),$$

we need some estimate of $(q_c^n(c))'$. By the equation $\hat{\phi}_c(q_c^n(c)) = (\hat{\Phi}(c))^{2^n} = t$, we have

$$\begin{aligned} (q_c^n(c))' &= \frac{\partial \hat{\phi}_c^{-1}}{\partial c}(t) + \frac{\partial \hat{\phi}_c^{-1}}{\partial t}(t) \cdot 2^n \cdot (\hat{\Phi}(c))^{2^n-1} \cdot \hat{\Phi}'(c) \\ &= \left(-\frac{1}{2t} + O(t^{-3})\right) + (1 + O(t^{-2})) \cdot 2^n \cdot \frac{t}{\hat{\Phi}(c)} \cdot \hat{\Phi}'(c) \end{aligned}$$

By applying the Cauchy integral formula to $\hat{\Phi}^{-1}$, we have

$$|\hat{\Phi}'(c)| \geq \frac{|\hat{\Phi}(c)| - 1}{r}.$$

Since $|t| = |\hat{\Phi}(c)|^{2^n} = R \gg 0$, it follows that

$$|(q_c^n(c))'| \geq C_0 \cdot 2^n R^{1-1/2^n} (R^{1/2^n} - 1)$$

for some constant $C_0 > 0$. In particular, the map $\hat{c} \mapsto q_c^n(\hat{c})$ is locally univalent near c . More precisely, there exists a maximal disk B of radius $\delta = \delta(c)$ centered at c where this map is univalent.

By the Koebe distortion theorem (see [6] for example), there exist uniform constants $C_1, C_2 > 0$ depending only on the value $|\hat{c} - c|/\delta$ such that

$$C_1 |(q_c^n(c))'| |\hat{c} - c| \leq |q_c^n(\hat{c}) - q_c^n(c)| \leq C_2 |(q_c^n(c))'| |\hat{c} - c|$$

for $\hat{c} \in B$, and $C_1, C_2 \rightarrow 1$ as $|\hat{c} - c|/\delta \rightarrow 0$. Hence by the inequality on the left we can take $\rho = |\hat{c} - c|$ as in the first estimate of the statement in order to have $|q_c^n(\hat{c}) - q_c^n(c)| > M/R$ when $R \gg 0$.

For the second estimate, recall that $|x|/2 \leq |e^x - 1| \leq 2|x|$ when $|x| \leq 1$. Now the estimate easily follows by setting $x := (\log R)/2^n$. \square

5.2.4. Possible improvement. We finish this subsection with a brief discussion on some possible improvement in errors. For calculation with less errors, we need to solve the equation $\hat{\phi}_c(q_c^n(c)) = t$ (or equivalently $q_c^n(c) = \hat{\phi}_c^{-1}(t)$) more precisely. We may improve the approximation of $\hat{\phi}_c(z)$ to degree 3, and consider the equation

$$\hat{\phi}_c(q_c^n(c)) \approx q_c^n(c) + \frac{c}{2q_c^n(c)} = t.$$

In this case, the Newton map is

$$N : c \mapsto c - \frac{2C_n^3 - 2tC_n^2 + cC_n}{2C_n^2D_n + C_n - cD_n},$$

where $C_n = q_c^n(c)$, $D_n = (q_c^n(c))'$.

Another way is that we may expand $\hat{\phi}_c^{-1}(t)$ as

$$\hat{\phi}_c^{-1}(t) = t - \frac{c}{2t} + \frac{c(3c-8)}{4t^3} + O\left(\frac{1}{t^5}\right)$$

when t is large enough. Then consider the Newton map

$$N : c \mapsto c - \frac{2tC_n - 2t^2 + c}{2tD_n - 1}$$

by using the approximation $q_c^n(c) = \hat{\phi}_c^{-1}(t) \approx t - c/(2t)$.

5.3. Comparison of the landing points obtained by the JES and OTIS algorithms. We spent 10 days by using a Dell OptiPlex GX620 machine to get the first 1000000 terms of the coefficients b_m . Let $P_N(w)$ be the partial sum

$$P_N(w) = w + \sum_{m=0}^N b_m w^{-m}$$

for $w \in \bar{\mathbb{D}}_1$.

Now that we have obtained the first one million terms of the coefficients, we are interested in knowing how the boundary ∂M_c of the Mandelbrot set M_c is approximated by them. Figure 5.1 illustrates the result by employing two kinds of distributed θ 's. In the figure, the one on the left side is depicted by

using 100000 evenly distributed w -points on the unit circle, i.e. $w = re^{i\frac{j*2\pi}{100000}}$, with $r = 1$ and $j = 0, 1, \dots, 100000$, while the other on the right is depicted by 100000 number of distinct w -points of the form $w = e^{i\frac{j*2\pi}{E}}$, where E is a prime number satisfying $E \leq 1153$ (the 191st prime), and $0 \leq j \leq E$. (When $E = 1153$, j is less than E so that the total number of w 's is 100000.)

In Figure 5.1 thick green curves depict the parameter rays of angles $1/6$, $5/12$ and $1/128$ obtained by the OTIS programme, whereas thin red curves represent the rays of same angles but computed by using the partial sum of (5.1) with the first one million terms. Direct inspection shows that these two curves of the same angle are very close to each other, and this fact can indeed readily be verified from Table 5.1, where the landing points of these two curves agree up to three decimal places.

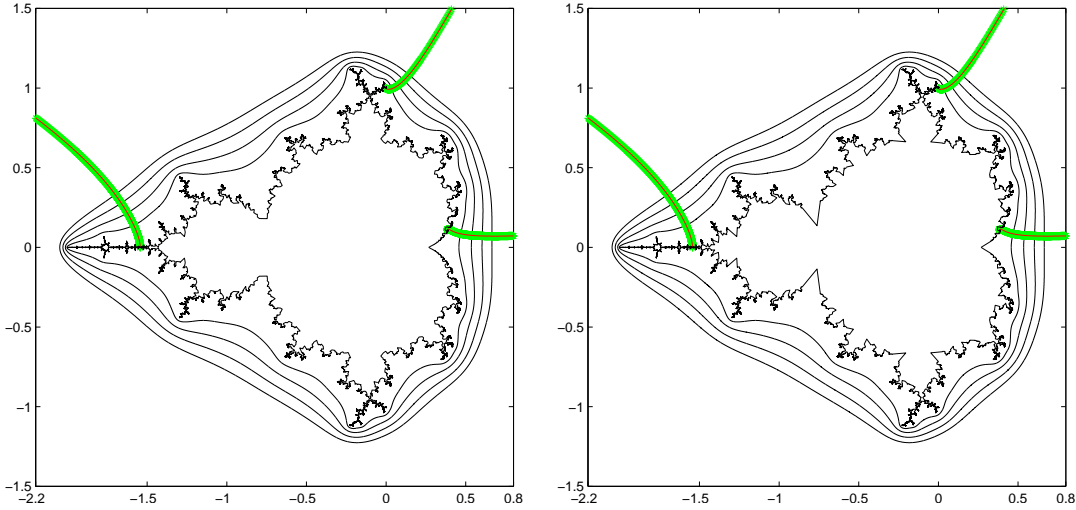


FIG. 5.1. Plots of the Mandelbrot set M_c , equipotential curves and external rays. The equipotential curves correspond to $r = 1$ (the ∂M_c case), 1.05, 1.10, 1.15, and 1.20. Colored curves show comparisons of the external rays of M_c for external angles $1/6$, $5/12$, and $1/128$ computed by means of Newton's method (the OTIS programme) and the Laurent series (the JES algorithm). (Note: the colored curves on both figures are the same.)

For given θ , in Table 5.1, $P_N(w)$ for $N = 999999$ means the numerical value of the landing point predicted by the JES algorithm, while the value obtained by the OTIS algorithm is indicated by $N = \text{OTIS}$. Theoretical value is shown by $N = \text{True}$. The parameters we used in the OTIS programme for this Table (and Table 5.2 as well) are: depth $D = 50$, sharpness $S = 200$, maximal radius $R = 1024$, number of iterations $L_m = 20$ for $1 \leq m \leq SD$. The theoretical values of the landing points of $\mathcal{R}(\theta; M_c)$ can be calculated by using the information of the binary representation of θ (see for example [6]): $1/2 \sim \{0\bar{1}\}$ thus its landing point is -2 ; $1/4 \sim \{01\bar{0}\}$ thus its landing point is a complex root of $c^3 + 2c^2 + 2c + 2 = 0$; $1/6 \sim \{00\bar{1}\}$ thus its landing point satisfies $c^2 + 1 = 0$; $1/8 \sim \{001\bar{0}\}$ and $3/8 \sim \{011\bar{0}\}$ thus their landing points are both a root of $q_c^2(c) - (1 + \sqrt{1 - 4c})/2 = 0$; $1/10 \sim \{000\bar{1}\}$ and $3/10 \sim \{0100\bar{1}\}$ thus their landing points both satisfy $q_c^4(c) + c = 0$; $1/12 \sim \{000\bar{1}\}$ and its landing point is a root of $q_c^3(c) - (-1 + i\sqrt{3 + 4c})/2 = 0$; $5/12 \sim \{011\bar{0}\}$ and its landing point fulfills $c^3 + 2c^2 + 2c + 2 = 0$; $1/128 \sim \{0000001\bar{0}\}$ thus its landing point is a root of $q_c^7(c) - (1 + \sqrt{1 - 4c})/2 = 0$.

In Table 5.2, we compare the landing points obtained by means of $P_{999999}(e^{i2\pi\theta})$ and of the OTIS programme with the theoretical values, when the denominators of the rational angles θ are odd. Using Schleicher's and the tuning algorithms [11, 12] together with the result of [29], we can determine the value of landing points or an equation for which the landing point of a rational parameter ray must satisfy. The formula for the landing point of angle $1/3 \sim \{0\bar{1}\}$ is $(1 - (e^{i2\pi \cdot 1/2} - 1)^2)/4$; $1/5 \sim \{00\bar{1}\}$ as so its landing point satisfies $64c^3 + 144c^2 + 108c + 135 = 0$; $2/5 \sim \{011\bar{0}\}$ as so its landing point satisfies

TABLE 5.1

Comparisons of the landing points of parameter rays $\mathcal{R}(\theta; M_c)$ of angles θ having even denominators.

$\theta = 1/2$		
N	$Re(P_N(w))$	$Im(P_N(w))$
4095	-2.000170	0.000000
8000	-1.999985	0.000000
240000	-2.000000	0.000000
499999	-2.000000	0.000000
999999	-2.000000	0.000000
True	-2	0
OTIS	-2.000000000	0.000000000

$\theta = 1/10$		
N	$Re(P_N(w))$	$Im(P_N(w))$
4095	0.384122	0.666625
8000	0.384085	0.666803
240000	0.384063	0.666806
499999	0.384064	0.666806
999999	0.384064	0.666806
True	0.384063957	0.666805123
OTIS	0.384063957	0.666805123

$\theta = 1/4$		
N	$Re(P_N(w))$	$Im(P_N(w))$
4095	-0.227985	1.115203
8000	-0.228169	1.115140
240000	-0.228156	1.115143
499999	-0.228155	1.115143
999999	-0.228155	1.115143
True	-0.228155494	1.115142508
OTIS	-0.228155494	1.115142508

$\theta = 3/10$		
N	$Re(P_N(w))$	$Im(P_N(w))$
4095	-0.564009	0.678968
8000	-0.564003	0.679479
240000	-0.564093	0.679279
499999	-0.564098	0.679266
999999	-0.564097	0.679266
True	-0.564097855	0.679273348
OTIS	-0.564097855	0.679273348

$\theta = 1/6$		
N	$Re(P_N(w))$	$Im(P_N(w))$
4095	-0.000149	1.000185
8000	-0.000071	1.000017
240000	0.000001	0.999999
499999	0.000000	1.000000
999999	0.000000	1.000000
True	0	1
OTIS	0.000000000	1.000000000

$\theta = 1/12$		
N	$Re(P_N(w))$	$Im(P_N(w))$
4095	0.419444	0.606297
8000	0.419567	0.606297
240000	0.419643	0.606290
499999	0.419643	0.606291
999999	0.419643	0.606291
True	0.419643378	0.606290729
OTIS	0.419643378	0.606290729

$\theta = 1/8$		
N	$Re(P_N(w))$	$Im(P_N(w))$
4095	0.343963	0.700579
8000	0.343995	0.700675
240000	0.343907	0.700621
499999	0.343907	0.700621
999999	0.343907	0.700620
True	0.343906996	0.700620020
OTIS	0.343906996	0.700620020

$\theta = 5/12$		
N	$Re(P_N(w))$	$Im(P_N(w))$
4095	-1.542516	0.000375
8000	-1.544201	0.000222
240000	-1.543648	0.000044
499999	-1.543713	0.000017
999999	-1.543674	0.000010
True	-1.543689013	0
OTIS	-1.543689012	0.000000000

$\theta = 3/8$		
N	$Re(P_N(w))$	$Im(P_N(w))$
4095	-1.296417	0.442035
8000	-1.296375	0.441823
240000	-1.296355	0.441851
499999	-1.296355	0.441852
999999	-1.296355	0.441852
True	-1.296355138	0.441851606
OTIS	-1.296355138	0.441851606

$\theta = 1/128$		
N	$Re(P_N(w))$	$Im(P_N(w))$
4095	0.379350	0.112366
8000	0.379729	0.108150
240000	0.385189	0.109403
499999	0.384934	0.109491
999999	0.384777	0.109466
True	0.384727430	0.109283294
OTIS	0.384727428	0.109283296

TABLE 5.2
 Comparisons of landing points of parameter rays $\mathcal{R}(\theta; M_c)$ of angles θ having odd denominators.

$\theta = 0$		
N	$Re(P_N(w))$	$Im(P_N(w))$
4095	0.288708	0.000000
8000	0.284608	0.000000
240000	0.270748	0.000000
499999	0.268911	0.000000
999999	0.267365	0.000000
True	0.25	0
OTIS	0.253924	0.000000

$\theta = 2/7$		
N	$Re(P_N(w))$	$Im(P_N(w))$
4095	-0.010385	0.682131
8000	-0.237317	0.679657
240000	-0.213615	0.666086
499999	-0.207707	0.665428
999999	-0.204842	0.662825
True	-0.125	0.649519053
OTIS	-0.161970	0.652518

$\theta = 1/3$		
N	$Re(P_N(w))$	$Im(P_N(w))$
4095	-0.779271	0.205335
8000	-0.769848	0.193527
240000	-0.764472	0.148521
499999	-0.761273	0.141574
999999	-0.762231	0.135394
True	-0.75	0
OTIS	-0.752446	0.063344

$\theta = 3/7$		
N	$Re(P_N(w))$	$Im(P_N(w))$
4095	-1.740300	0.004782
8000	-1.742037	0.002802
240000	-1.745167	0.001499
499999	-1.745843	0.001077
999999	-1.746073	0.000835
True	-1.75	0
OTIS	-1.749219	0.000080

$\theta = 1/5$		
N	$Re(P_N(w))$	$Im(P_N(w))$
4095	-0.145897	1.031616
8000	-0.147312	1.030741
240000	-0.151132	1.030247
499999	-0.151595	1.030258
999999	-0.151559	1.030489
True	-0.154724606	1.031047228
OTIS	-0.154174	1.030811

$\theta = 1/9$		
N	$Re(P_N(w))$	$Im(P_N(w))$
4095	0.361998	0.685793
8000	0.361762	0.685466
240000	0.360800	0.685051
499999	0.360739	0.684965
999999	0.360665	0.684903
True	0.360029616	0.684763498
OTIS	0.360126	0.684774

$\theta = 2/5$		
N	$Re(P_N(w))$	$Im(P_N(w))$
4095	-1.285488	0.103334
8000	-1.275531	0.096360
240000	-1.266109	0.075502
499999	-1.265969	0.069374
999999	-1.265788	0.067670
True	-1.25	0
OTIS	-1.253231	0.031539

$\theta = 2/9$		
N	$Re(P_N(w))$	$Im(P_N(w))$
4095	-0.165055	1.098278
8000	-0.164627	1.098236
240000	-0.164125	1.097907
499999	-0.164038	1.097879
999999	-0.163964	1.097844
True	-0.163657004	1.097773914
OTIS	-0.163701	1.097775

$\theta = 1/7$		
N	$Re(P_N(w))$	$Im(P_N(w))$
4095	-0.010385	0.682131
8000	-0.014153	0.676970
240000	-0.040882	0.666103
499999	-0.043847	0.664666
999999	-0.047989	0.662083
True	-0.125	0.649519053
OTIS	-0.088628	0.652513

$\theta = 4/9$		
N	$Re(P_N(w))$	$Im(P_N(w))$
4095	-1.774298	0.014378
8000	-1.772787	0.012993
240000	-1.771548	0.009310
499999	-1.770902	0.008594
999999	-1.770345	0.008319
True	-1.768529152	0
OTIS	-1.768986	0.003490

TABLE 5.3

A_{4095}	A_{8000}	A_{240000}	A_{342000}	A_{470000}	A_{499999}	A_{999999}
1.834525	1.807288	1.727439	1.719775	1.714209	1.713306	1.703927

$4c + 5 = 0$; for both angles $1/7 \sim \{\overline{001}\}$ and $2/7 \sim \{\overline{010}\}$ the formulae are $(1 - (e^{i2\pi \cdot 1/3} - 1)^2)/4$; $3/7 \sim \{\overline{011}\}$ thus its landing point fulfills $4c + 7 = 0$; $4/9 \sim \{\overline{011100}\}$ as so its landing point fulfills $64c^3 + 128c^2 + 72c + 81 = 0$; the exact values of the landing points of parameter rays of angles $1/9 \sim \{\overline{000111}\}$ and $2/9 \sim \{\overline{001110}\}$ are two roots of a 20-degree polynomial that can be found in Table 1 of [29].

Remark 5.3. The parameters used in the OTIS programme for Table 5.2 are the same as those in Table 5.1. In the Table 5.2 case, the dynamics of q_c with the landing point c has a parabolic cycle, and the convergence of $\hat{\Phi}^{-1}(re^{2\pi i\theta}) \rightarrow c$ as $r \rightarrow 1^+$ is quite slow. To improve the error of OTIS in Table 5.2 we need to increase the depth of the approximating ray.

We end this article by addressing the area of the Mandelbrot set M_c . Taking advantage of the one million coefficients, we incidentally find a new upper bound for the area. Recall that the area is given by $A_\infty := \lim_{N \rightarrow \infty} A_N$, namely Gronwall's area formula, where

$$A_N = \pi \left(1 - \sum_{m=1}^N m |b_m|^2 \right).$$

Table 5.3 shows the values of A_N for seven number of N 's. The first 4095 coefficients were achieved in [20]; the first 8000 coefficients were used in [2]. In [18], A_{240000} was firstly obtained. It was also suggested that A_∞ is between 1.66 and 1.71. On the other hand, notice that all estimates of the area of M_c obtained by "pixel counting" in [18] appear to be no larger than 1.53.

Acknowledgments. Y-C Chen was supported by NSC 96-2115-M-001-007 and NSC 97-2119-M-001-008. He is grateful to Mitsuhiro Shishikura for bringing the work [4] into his attention, and to Robert L Devaney for discussing the work [4]. He thanks Nagoya University and Tokyo Metropolitan University for hospitality during his visits. T Kawahira would like to thank Academia Sinica for their support and hospitality. He was also partially supported by JSPS Grant-in-Aid for Scientific Research. J-M Yuan was supported by NSC 97-2115-M-126-001. A portion of this work was done when he was visiting Academia Sinica.

REFERENCES

- [1] S. AUBRY AND G. ABRAMOVICI, *Chaotic trajectories in the standard map: the concept of anti-integrability*, Physica D, 43 (1990), pp. 199–219.
- [2] B. BIELEFELD, Y. FISHER AND F. V. HAESELER, *Computing the Laurent series of the map $\Psi: C - \overline{D} \rightarrow C - M$* , Adv. Appl. Math., 14 (1993), pp. 25–38.
- [3] P. BLANCHARD, *Complex analytic dynamics on the Riemann sphere*, Bull. Amer. Math. Soc. (N.S.), 11 (1984), pp. 85–141.
- [4] P. BLANCHARD, R. L. DEVANEY AND L. KEEN, *The dynamics of complex polynomials and automorphisms of the shift*, Invent. Math., 104 (1991), pp. 545–580.
- [5] R. BROOKS AND J. P. MATELSKI, *The dynamics of 2-generator subgroups of $\text{PSL}(2, C)$* , in Riemann surfaces and related topics: Proceedings of the 1978 Stony Brook Conference, Ann. of Math. Stud., 97, Princeton Univ. Press, Princeton, N.J., 1981, pp. 65–71.
- [6] L. CARLESON AND T. W. GAMELIN, *Complex Dynamics*, Springer-Verlag, New York, 1993.
- [7] Y.-C. CHEN, *Bernoulli shift for second order recurrence relations near the anti-integrable limit*, Discrete Contin. Dyn. Syst. B, 5 (2005), pp. 587–598.
- [8] Y.-C. CHEN, *Anti-integrability for the logistic maps*, Chinese Ann. Math. B, 28 (2007), pp. 219–224.
- [9] Y.-C. CHEN, *Family of invariant Cantor sets as orbits of differential equations*, Int. J. Bifurcat. Chaos, 18 (2008), pp. 1825–1843.
- [10] R. L. DEVANEY, *An Introduction to Chaotic Dynamical Systems*, 2nd Ed, Addison-Wesley Pub. Co. 1989.

- [11] R. L. DEVANEY, *The complex dynamics of quadratic polynomials*, in Complex Dynamical Systems, Proc. Sympos. Appl. Math., 49, Amer. Math. Soc., Providence, RI, 1994, pp. 1–29.
- [12] A. DOUADY, *Algorithms for computing angles in the Mandelbrot set*, in Chaotic Dynamics and Fractals, Notes Rep. Math. Sci. Engrg., 2, Academic Press, Orlando, FL, 1986, pp. 155–168.
- [13] A. DOUADY, *Does a Julia set depend continuously on the polynomial?*, in Complex Dynamical Systems, Proc. Sympos. Appl. Math., 49, Amer. Math. Soc., Providence, RI, 1994, pp. 91–138.
- [14] A. DOUADY AND J. H. HUBBARD, *Iteration des polynomes quadratiques complexes*, C. R. Acad. Sci. Paris Ser. I Math., 294 (1982), pp. 123–126.
- [15] A. DOUADY AND J. H. HUBBARD, *Etude dynamique des polynomes complexes. Partie I*, Publications Mathematiques d'Orsay, 84-2, 1984.
- [16] J. H. EWING AND G. SCHOBER, *On the coefficients of the mapping to the exterior of the Mandelbrot set*, Michigan Math. J., 37 (1990), pp. 315–320.
- [17] J. H. EWING AND G. SCHOBER, *Coefficients associated with the reciprocal of the Mandelbrot set*, J. Math. Anal. Appl., 170 (1992), pp. 104–114.
- [18] J. H. EWING AND G. SCHOBER, *The area of the Mandelbrot set*, Numer. Math., 61 (1992), pp. 59–72.
- [19] P. HENRICI, *Elements of Numerical Analysis*, Wiley, 1964.
- [20] I. JUNGREIS, *The uniformization of the complement of the Mandelbrot set*, Duke Math. J., 52 (1985), pp. 935–938.
- [21] T. KAWAHIRA, *OTIS*, Java applet, available online at <http://www.math.nagoya-u.ac.jp/~kawahira/programs/otis.html>.
- [22] M. LYUBICH, *Some typical properties of the dynamics of rational mappings*, Russian Math. Surveys, 38 (1983), pp. 154–155.
- [23] R. S. MACKAY AND J. D. MEISS, *Cantori for symplectic maps near the anti-integrable limit*, Nonlinearity, 5 (1992), pp. 149–160.
- [24] B. MANDELBROT, *Fractal aspects of the iteration of $z \mapsto \lambda z(1 - z)$ for complex λ and z* , Annals of New York Academy of Science, 357 (1980), pp. 249–259.
- [25] R. MAÑÉ, P. SAD, AND D. SULLIVAN, *On the dynamics of rational maps*, Ann. Sci. Ecole Norm. Sup., (4) 16 (1983), pp. 193–217.
- [26] J. MILNOR, *Periodic orbits, external rays and the Mandelbrot set: an expository account*, Geometrie complexe et systemes dynamiques, Asterisque, 261 (2000), pp. 277–333.
- [27] J. MILNOR, *Dynamics in One Complex Variable*, 3rd ed., Annals of Mathematics Studies, 160, Princeton University Press, Princeton, NJ, 2006.
- [28] S. MOROSAWA, Y. NISHIMURA, M. TANIGUCHI AND T. UEDA, *Holomorphic Dynamics*, Cambridge University Press, Cambridge, 2000.
- [29] P. MORTON AND F. VIVALDI, *Bifurcations and discriminants for polynomial maps*, Nonlinearity, 8 (1995), pp. 571–584.
- [30] D. STERLING AND J. D. MEISS, *Computing periodic orbits using the anti-integrable limit*, Phys. Lett. A 241 (1998), pp. 46–52.